Extending the SAFT-γ Mie approach to model benzoic acid, diphenylamine, and mefenamic acid: solubility prediction and experimental measurement

Sara A. Febra[a,b], Thomas Bernet[a], Corin Mack[c,e], John McGinty[c,d], Iyke I. Onyemelukwe[c], Stephanie J. Urwin[c], Jan Sefcik[c,d], Joop H. ter Horst[c,e], Claire S. Adjiman[a], George Jackson[a], Amparo Galindo[a,*]

[a] *Department of Chemical Engineering, Centre for Process Systems Engineering, Institute for Molecular Science and Engineering, Imperial College London, South Kensington Campus, London SW7 2AZ, United Kingdom*
[b] *Current address: Equinor ASA, 1330 Fornebu, Norway*
[c] *Future Manufacturing Research Hub in Continuous Manufacturing and Advanced Crystallisation, Technology and Innovation Centre, University of Strathclyde, 99 George Street, Glasgow G1 1RD, United Kingdom*
[d] *Department of Chemical and Process Engineering, University of Strathclyde, James Weir Building, 75 Montrose Street, Glasgow G1 1XJ, United Kingdom*
[e] *Strathclyde Institute of Pharmacy and Biomedical Sciences (SIPBS), University of Strathclyde, 161 Cathedral St, Glasgow G4 0RE, United Kingdom*

Abstract

The prediction of the solubility of pharmaceutical ingredients (APIs) is a significant challenge of interest in pharmaceutical applications and solvent selection processes. Here, we extend the table of group-group interactions (3 like interactions, 47 unlike interactions) of the SAFT-γ Mie group-contribution equation of state to model the phase behaviour and solubility of mefenamic acid, a nonsteroidal anti-inflammatory drug, in a range of solvents. In addition to mefenamic acid, we also consider its molecular synthons: benzoic acid and diphenylamine. New experimental solubility data are presented for the three molecules in a range of solvents, and three new SAFT-γ Mie groups are defined (aCCOOH, aCNHaC and CH_3CO) and characterised, together with their unlike interactions with solvent groups. Literature data of vapour pressure, single-phase density, saturation density, vapourisation enthalpy, bubble temperature, dew tempera-

*Corresponding author
Email address: a.galindo@imperial.ac.uk (Amparo Galindo)

ture, and bubble pressure are used to characterise the new group-group interactions. Solubility data are used to characterise the new group-group interactions only if there are no other experimental data available. The transferability and predictive accuracy of the new models are assessed by comparison of the theoretical predictions with the experimental solubility data. Our comparison includes alcohols, ketones, and esters as families of solvents and includes mixed-solvent solubility predictions.

Keywords: statistical associating fluid theory (SAFT), mefenamic acid, solubility, group contribution

1. Introduction

The development of pharmaceutical drugs and biomedical applications requires the knowledge of the thermodynamic properties of mixtures involving active pharmaceutical ingredients (APIs) and solvents. In particular, the solubility of solid APIs in liquids, together with permeability, is a key property determining bioavailability, as well as dictating early on the choice of reaction solvents and separation processes (typically crystallisation), the final formulation of the drug, and its manufacturing method. As such, a considerable amount of experimental work is currently expended in screening solvents and solvent mixtures for optimal drug solubility [1], a process that can be time-consuming, and often ineffective, as only a relative small number of API-solvent combinations can be practically screened.

Mefenamic acid (2-[(2,3-dimethylphenyl)amino]benzoic acid; $C_{15}H_{15}NO_2$; CAS number: [61-68-7]) is a nonsteroidal anti-inflammatory drug (NSAID) and analgesic, used to treat moderate pain [2, 3, 4]. Mefenamic acid is known to crystallise in two forms (Form I and Form II) [5, 6, 7, 8], and a Form III has recently been reported [9]. Form I is stable at ambient conditions with respect to Forms II and III, and is interesting to note that at higher temperatures the order of stability changes to II>I>III. In a number of studies the existence of the different crystal forms crystallised from a variety of solvents is presented [8, 10].

The existence of different forms affects the crystallisation in pharmaceutical processes [11, 12]. Although the metastable forms are expected to be more pharmaceutically active, because of their higher solubility, it is more practical for pharmaceutical formulations to consider the stable Form I. In a number of previous works the solubility of Form I has been reported, in ethanol and octan-1-ol [13, 14] and carbon dioxide [15]. Mudalip et al. [16] report high solubility of mefenamic acid (Form I) in dipolar aprotic solvents, moderate in polar protic ones, and poor solubility in non-polar aprotic solvents and in water.

The development of theoretical methods that can accurately predict solubility, as well as other thermodynamic properties, can be helpful in reducing the number of experiments needed. Specifically, theoretical approaches that are based on statistical mechanics stemming from a detailed description of the molecular system at the microscopic scale, are relevant in this context. The API + solvent systems, involve wide range complex intermolecular interactions that need to be taken into account in order for the model to deliver sufficient accuracy.

In particular, molecular equations of state (EoSs) are very useful tools for the prediction of thermodynamic properties of complex mixtures. The statistical associating fluid theory (SAFT) [17, 18] in particular is a molecular EoS that can be used to model complex molecules, including the molecules that exhibit hydrogen bonding. In the original version of SAFT [17, 18] molecules are treated as homonuclear chains of tangentially bonded spherical segments in which associating sites mediate directional interactions that mimic hydrogen bonds [19, 20]. The spherical segments forming the model molecules interact through a specified pair potential: a Lennard-Jones potential treated as a temperature-dependent hard-sphere and dispersion interactions in the original version of the approach [17, 18]; a square-well potential in the SAFT-VR model [21]; a Lennard-Jones potential implemented using computer simulation data in soft-SAFT [22, 23, 24, 25, 26]; and more recently a Mie potential (a generalised Lennard-Jones potential) in SAFT-VR Mie [27].

A slightly different perturbation is followed in the PC-SAFT approach [28]

and in its extension to charged molecules, ePC-SAFT [29]; in these a reference chain fluid is used. PC-SAFT and ePC-SAFT provide accurate results [30] and have been applied for the prediction the solubility of a large number of compounds [31, 32, 33], and in studies including pH effects [34, 35], in systems including APIs, polymers, and amorphous formulations [36, 37, 38, 39, 40] in recent works.

The incorporation of a Mie potential in the SAFT-VR framework [27] and the implementation of a third-order high-temperature expansion lead to a very accurate equation of state, capable of delivering accurate derivative properties (a stringent test to the accuracy of any given model). Of interest here is the recasting of SAFT-VR Mie as a group-contribution approach in the SAFT-γ Mie equation of state [41, 42, 43]. The method, has been shown to retain the accuracy of the molecular approach and to be accurate for the prediction of a broad range of equilibrium thermodynamic properties, including vapour-liquid, liquid-liquid and solid-liquid phase equilibria, as well as single phase and derivative properties. Furthermore, the approach can be used to develop SAFT-γ transferable force-field parameters for use in molecular simulations [44]. An update of the current capabilities of the method and the group interactions available can be found in ref. [43]. In particular, octanol-water partition coefficients for a range of APIs are predicted in ref. [45], and in ref. [46] aqueous mixtures of choline and geranate (CAGE), a mixture shown to exhibit therapeutic properties, are modelled. In our current work we extend the applicability of the approach in pharmaceutically relevant systems by considering mefenamic acid and related molecules in a range of solvents.

Here, we present new solubility data for Form I of mefenamic acid, benzoic acid and diphenylamine, in a range of alcohols, ketones and esters, as well as for benzoic acid and diphenylamine. Moreover, the data measured in our current work is useful for the development and assessment of the SAFT-γ group contribution equation of state, and serves a test of the predictive ability of the method. The thermodynamic modelling of mefenamic acid with SAFT-γ Mie requires the definition and the characterisation of new groups. Mefenamic

acid is composed of two phenyl rings bound by an amine group, a carboxyl group bound to one of the two phenyl rings, and two methyl groups bound to the other phenyl ring. In terms of developing a SAFT-γ Mie model for these molecules, the contribution of each group can be considered separately following the group-contribution premise. We hence also present solubility measurements for benzoic acid and diphenylamine in a range of solvents, as these molecules incorporate relevant moieties for mefenamic acid. Furthermore, a number of other NSAIDs, e.g., fenamic, tolfenamic, flufenamic, and meclofenamic acids, are similarly composed of a carboxyl, an amine, and two phenyl groups, with a structure similar to that of mefenamic acid. The development of new SAFT-γ Mie groups relevant to mefenamic acid will also be transferable to these.

In Section 2, the experimental methodology and SAFT-γ Mie model are presented. In Section 3, the experimental measurements of the melting properties of benzoic acid, diphenylamine and mefenamic acid are presented, together with the measured solubilities and activity coefficients in a large range of solvents. The results of SAFT-γ Mie are also detailed in Section 3, where we present the estimated parameters of the new group-group interactions, together with the predictions of solubility. Final remarks are provided in section 4

2. Methods

2.1. Experimental materials and methodology

Materials. Mefenamic acid (98%), benzoic acid (99%), and diphenylamine (98%) (Fig. 1) were supplied by Sigma Aldrich (MerkKGaA, Germany), with the polymorphic forms supplied all being of their stable form. The solvents used are listed in Table 1.

Solubility.

Sample preparation. A known amount of one of the crystalline materials was weighed into a 1.5 ml high-performance liquid chromatography (HPLC) vial. 1 ml of a specific solvent was then pipetted into this pre-weighed vial

Table 1: The solvents used within this study with their molecular weights (MW).

Solvent	Purity / %	MW / (g/mol)	Supplier
ethanol	99	46.1	VWR
propan-1-ol	99	60.1	VWR
butan-1-ol	99	74.1	VWR
butan-2-ol	99	74.1	VWR
pentan-2-ol	99	88.2	VWR
2-methyl-1-propanol	99	74.1	VWR
3-methyl-1-butanol	99	88.1	VWR
acetone	99	58.1	VWR
butan-2-one	99	72.1	VWR
pentan-2-one	99	86.13	VWR
heptan-2-one	99	114.2	VWR
methyl isobutyl ketone	98	110.2	VWR
ethyl acetate	99	88.1	VWR
propyl acetate	99	102.1	VWR
butyl acetate	99	116.2	VWR
isopropyl acetate	99	102.1	VWR
isobutyl acetate	99	116.2	VWR
1,2-dimethylcyclohexane	98	112.1	Sigma-Aldrich

containing the solid material and stirrer bar. The vial was then reweighed in order to determine the exact mass of solvent added and therefore the exact molar composition of the sample. Due high solubility of some combinations of model compound and solvent, the amount of solvent added was reduced in some cases. Each vial was capped tightly and the cap was carefully wrapped in parafilm tape to create a seal and prevent solvent loss at high temperatures. The overall weight (mg) of the sealed vial containing the solvent, stirrer, and solid material was recorded to check for weight loss after solubility measurements in the Crystal16.

The model compounds were not purified further. The solids were gently milled in order to create a fine powder for easier initial dissolution. As we recrystallize the solid initially present in the sample before we determine the clear-point temperature the initially present solid form is not important for the measurement. Still, milling was checked to have no impact on polymorphic form. The crystal form of mefenamic acid after milling was confirmed by Fourier-transform infrared (FTIR) spectroscopy analysis. We also checked the final solid form using FTIR which is explained later on in the paper (Section 2.1).

Solubility measurement. The Crystal16 Multiple Reactor (Technobis Crystallization Systems, The Netherlands) was used to determine the saturation temperature for each prepared sample, similarly to the method utilized by Reus *et al.* [47]. When solids are present in the vial, the transmission of light through the vial is hindered by the stirring suspension, whereas in the absence of particles the light passes unhindered. To dissolve the particles in the stirred (700–1000 rpm) suspension, a heating rate of 0.2 K/min was applied up to a pre-set high temperature.

By cooling the solution (0.4 K/min) to a pre-set low temperature, the solubility of the solute in the solution decreases and at some point the sample recrystallized. Temperature was kept constant for 30 minutes at both the pre-set low and high temperature to ensure adequate dissolution and recrystallization. The pre-set high and low temperature in a temperature profile were adjusted in subsequent temperature cycles for time efficiency and increased experiment success rate. The pre-set high temperature is 353 K. For solvents with a boiling point less than 353 K the pre-set high temperature was chosen to be 10 K under the boiling temperature with a maximum of 353 K. The pre-set low temperature was chosen to be 273 K. After each cycle the set high temperature was automatically adjusted to 10 K higher than the highest saturation temperature measured in the previous cycles, with a maximum of 353 K. The set low temperature was automatically adjusted to induce crystallization during cooling instead of during the hold step, with a minimum of 283 K. The low

temperature in subsequent cycles was for instance increased with benzoic acid and mefenamic acid as crystallization initiated with only slight undercooling. For accuracy, four temperature cycles were performed. The first temperature cycle was used to calibrate 100% transmission of the clear solution at a pre-set high temperature. In the three subsequent temperature cycles the clear-point temperature was determined as the temperature at which, upon heating, the transmission of light reached 100%. The average of the clear-point temperatures was taken as the saturation temperature for the composition in the vial. To save measurement time, the pre-set high and low temperatures of subsequent cycles were adjusted accordingly depending on the preceding clear and cloud point measured from the first cycle and the boiling point of the solvent, thus ensuring complete dissolution of the solute and reduced time frames.

Solid product analysis.

Differential Scanning Calorimetry (DSC) analysis. DSC (Polyma DSC 214, Netzsch) was carried out in order to determine the melting temperature T_i^{fus} and melting enthalpy $\Delta h_i^{\mathrm{fus}}$, where i denotes the species (benzoic acid, diphenylamine, or mefenamic acid). A small amount (< 5 mg) of a specific compound is weighed into a metal DSC pan and sealed. A heating rate of 10 K/min [48, 49] from 298 K up to 498 K was used. The onset of the endotherm was taken as the melting temperature and the integrated endotherm was taken as the melting enthalpy of the measured compound. In order to assess variation in melting temperature and melting enthalpy measurements, multiple samples were measured, with the resulting values averaged yielding a specific value for each and a respective error.

Fourier-transform infrared (FTIR) spectroscopy analysis. The Tensor II FTIR spectrometer (Bruker, Germany) was used to check the polymorph present at the end of the solubility measurement in the suspension in the low temperature region of the temperature cycle. Samples were removed from the

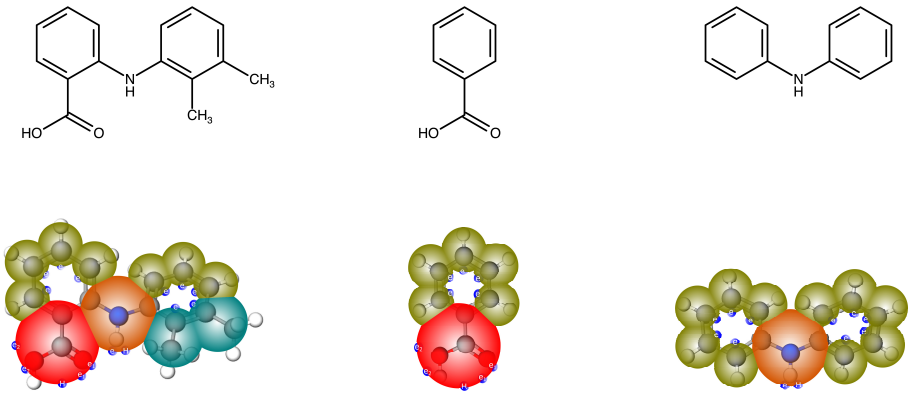

(a) (b) (c)

Figure 1: Skeletal formula and SAFT-γ Mie molecular modelling of: (a) mefenamic acid (MW_{MFA} = 241.3 g/mol); (b) benzoic acid (MW_{BA} = 112.1 g/mol); (c) diphenylamine (MW_{DPA} = 169.2 g/mol). Mefenamic acid is modelled by a combination of one aCCOOH, one aCNHaC, seven aCH, and two aCCH$_3$ groups. Benzoic acid is modelled with six aromatic carbon aCH groups, and one aCCOOH group, while dyphenilamine includes ten aCH groups, and one aCNHaC group. Association sites are denoted by the smaller blue circles, labelled e for electronegative (acceptor) sites and H for hydrogen (donor) sites.

Crystal16 setup and the solids were vacuum filtered, washed with their respective solvent to ensure the mother liquor had been removed and dried in air for 3 days. Due to the low volatility of some of the solvents, some samples were placed in an in-house oven set at 308 K until fully dry. The dried samples were then placed on the FTIR for measurement. The IR spectra was analysed over a wavenumber range of 400–4000 cm^{-1}. Each sample was measured twice to confirm the validity of the measured spectra. No difference in the polymorphic form was detected between the stable form supplied and the recrystallized samples.

2.2. SAFT-γ Mie model and theory

In the SAFT-γ Mie approach [41, 50] molecules are represented as associating heteronuclear chains of fused spherical segments that interact through Mie potentials of variable range. Short-range directional interactions are added by embedding square-well association sites on any given segment. The total

Helmholtz free energy A of a mixture of non-ionic species is expressed as the sum of four contributions:

$$A = A^{\text{ideal}} + A^{\text{monomer}} + A^{\text{chain}} + A^{\text{association}}, \tag{1}$$

where A^{ideal} is the ideal free energy of the mixture, A^{monomer} is the contribution accounting for the Mie segment-segment interactions, A^{chain} is the free energy associated with the formation of chains, and $A^{\text{association}}$ is the contribution to the free energy due to association. Detailed expressions for each of the free energy terms can be found in [41, 42, 50, 51]

Following the group-contribution premise, molecules are modelled as partitioned into functional groups, and it is assumed that the properties of a given molecule (or mixture) can be obtained by accounting for the appropriate contributions of the groups. The parameters characterising any given group are treated as transferable to other molecules and mixtures which contain the same group. The SAFT-γ Mie representation of benzoic acid, diphenylamine and mefenamic acid can be seen in Figure1. A given group k incorporates a number of ν_k^* identical spherical segments, and a shape factor S_k ($0 \leq S_k \leq 1$), characterizing the contribution of a segment to the overall molecular properties of the molecule. The interaction between two segments of groups k and l is described through a Mie potential

$$\phi_{kl}^{\text{Mie}}(r_{kl}) = \mathcal{C}_{kl}\varepsilon_{kl}\left[\left(\frac{\sigma_{kl}}{r_{kl}}\right)^{\lambda_{kl}^r} - \left(\frac{\sigma_{kl}}{r_{kl}}\right)^{\lambda_{kl}^a}\right] \tag{2}$$

where r_{kl} is the distance between the centers of the two segments, σ_{kl} the segment diameter, ε_{kl} the depth of the potential well, and λ_{kl}^r and λ_{kl}^a the repulsive and attractive exponents of the Mie potential, respectively. The prefactor $\mathcal{C}_{kl}$ ensures that the minimum of interaction is $-\varepsilon_{kl}$, and is a function of the exponents, as

$$\mathcal{C}_{kl} = \frac{\lambda_{kl}^r}{\lambda_{kl}^r - \lambda_{kl}^a}\left(\frac{\lambda_{kl}^r}{\lambda_{kl}^a}\right)^{\frac{\lambda_{kl}^a}{\lambda_{kl}^r - \lambda_{kl}^a}}. \tag{3}$$

Hydrogen bonding and strong polar interactions are represented by short-ranged square-well association sites, placed on the segments. $N_{\text{ST},k}$ is the number of

different association site types for a group k, and $n_{k,a}$ the number of sites of a given type $a = 1, \ldots, N_{\mathrm{ST},k}$. The interaction between a site of type a placed on a segment of type k and a site of type b placed on a segment of type l is given by

$$\phi^{\mathrm{HB}}_{kl,ab}(r_{kl,ab}) = \begin{cases} -\varepsilon^{\mathrm{HB}}_{kl,ab} & \text{if } r_{kl,ab} \leq r^{\mathrm{c}}_{kl,ab} \\ 0 & \text{if } r_{kl,ab} > r^{\mathrm{c}}_{kl,ab} \end{cases} \tag{4}$$

where $r_{kl,ab}$ is the distance between the centers of the two sites, $\varepsilon^{\mathrm{HB}}_{kl,ab}$ the association energy, and $r^{\mathrm{c}}_{kl,ab}$ the cutoff range of the interaction. The site a is positioned at distance $r^{\mathrm{d}}_{kk,aa}$ from the center of the segment k, and the site b is positioned at distance $r^{\mathrm{d}}_{ll,bb}$ from the center of the segment l. The range of the association can equivalently be described by the cutoff $r^{\mathrm{c}}_{kl,ab}$, or by the bonding volume $K^{\mathrm{HB}}_{kl,ab}$, for given $r^{\mathrm{d}}_{kk,aa}$ and $r^{\mathrm{d}}_{ll,bb}$.

The interactions between groups k and l involve unlike parameters, which can be obtained through combining rules (CR) in first instance. The unlike segment diameter is obtained from a Lorentz-like arithmetic mean of the like diameters, as

$$\sigma_{kl} = \frac{\sigma_{kk} + \sigma_{ll}}{2}. \tag{5}$$

The unlike exponents λ^r_{kl} and λ^a_{kl}, and the unlike dispersion energy ε_{kl} can be obtained by a Berthelot-like geometric mean rule, as

$$\lambda^x_{kl} = 3 + \sqrt{(\lambda^x_{kk} - 3)(\lambda^x_{ll} - 3)} \tag{6}$$

where $x = (r, a)$, and

$$\varepsilon_{kl} = \frac{\sqrt{{\sigma_{kk}}^3 {\sigma_{ll}}^3}}{{\sigma_{kl}}^3} \sqrt{\varepsilon_{kk}\varepsilon_{ll}}, \tag{7}$$

which accounts for differences in the size of the segments. Similar arithmetic and geometric rules can be used to obtain the bonding volume $K^{\mathrm{HB}}_{kl,ab}$ and the association energy parameter $\varepsilon^{\mathrm{HB}}_{kl,ab}$ between unlike sites, as

$$K^{\mathrm{HB}}_{kl,ab} = \left(\frac{\sqrt[3]{K^{\mathrm{HB}}_{kk,aa}} + \sqrt[3]{K^{\mathrm{HB}}_{ll,bb}}}{2} \right)^3 \tag{8}$$

and

$$\varepsilon^{\mathrm{HB}}_{kl,ab} = \sqrt{\varepsilon^{\mathrm{HB}}_{kk,aa}\varepsilon^{\mathrm{HB}}_{ll,bb}}. \tag{9}$$

The combining rules are employed to obtain a first estimate of the unlike parameters. In practice, however, ε_{kl}, λ^x_{kl}, $K^{\mathrm{HB}}_{kl,ab}$, and $\varepsilon^{\mathrm{HB}}_{kl,ab}$ are typically estimated by comparison to target experimental thermophysical properties of pure fluids or mixtures in which the functional group is present.

The equilibrium thermodynamic properties of the fluid can be determined from the total Helmholtz free energy A at temperature T, volume V, and vector number $\boldsymbol{N}$ of molecules, which is composed of elements N_i of compounds i, such that $N = \sum_i N_i$. The pressure is given by

$$P = -\left(\frac{\partial A}{\partial V}\right)_{T,N}, \tag{10}$$

and the chemical potential of a compound i by

$$\mu_i = \left(\frac{\partial A}{\partial N_i}\right)_{T,V,N_{j\neq i}}. \tag{11}$$

These standard relations can be used to determine fluid phase-equilibrium conditions, e.g., vapour pressure P^{sat} and saturated liquid density ρ_l^{sat}.

2.3. Solid-liquid equilibria

The solubility of a compound i in a given solvent at a given temperature T and pressure P can be defined by its molar fraction $\boldsymbol{x}^{\mathrm{sat}}$ in the saturated solution. It is an equilibrium property, characterised by the equality between the chemical potential of the solid phase (S), assumed pure here, and the chemical potential of the liquid phase (L), as

$$\mu_i^{\mathrm{S}}(T, P, x_i^{\mathrm{S}} = 1) = \mu_i^{\mathrm{sat}}(T, P, \boldsymbol{x}^{\mathrm{sat}}). \tag{12}$$

The activity of the compound in solution $a_i^{\mathrm{sat}}(T, P, \boldsymbol{x}^{\mathrm{sat}})$ is related to the partial molar Gibbs free energy of fusion of pure i, $\Delta g_i^{\mathrm{fus}}(T, P)$ as

$$\ln a_i^{\mathrm{sat}}(T, P, \boldsymbol{x}^{\mathrm{sat}}) = -\frac{\Delta g_i^{\mathrm{fus}}(T, P)}{RT}, \tag{13}$$

where R is the molar gas constant. The Gibbs free energy of fusion can be expressed in terms the fusion enthalpy $\Delta h_i^{\mathrm{fus}}(T, P)$ and entropy $\Delta s_i^{\mathrm{fus}}(T, P)$ from

the classic relation $\Delta g_i^{\mathrm{fus}}(T,P) = \Delta h_i^{\mathrm{fus}}(T,P) - T\Delta s_i^{\mathrm{fus}}(T,P)$. The temperature T of the system is below the fusion temperature T_i^{fus} of compound i, since the phase L corresponds to a solution. The fusion enthalpy $\Delta h_i^{\mathrm{fus}}$ and entropy $\Delta s_i^{\mathrm{fus}}$ at arbitrary $T < T_i^{\mathrm{fus}}$ and P are generally unknown experimentally, but can be expressed from their values at the fusion temperature T_i^{fus} and ambient pressure P_{amb}.

By assuming that the solution is incompressible, and neglecting pressure effects, $\Delta h_i^{\mathrm{fus}}(T,P)$ and $\Delta s_i^{\mathrm{fus}}(T,P)$ can be expressed as

$$\begin{aligned} \Delta h_i^{\mathrm{fus}}(T,P) = \quad & \Delta h_i^{\mathrm{fus}}(T_i^{\mathrm{fus}},P) \\ & - \int_T^{T_i^{\mathrm{fus}}} \Delta c_{p,\,i}(T',P)\, dT', \end{aligned} \tag{14}$$

and

$$\begin{aligned} \Delta s_i^{\mathrm{fus}}(T,P) = \quad & \Delta s_i^{\mathrm{fus}}(T_i^{\mathrm{fus}},P) \\ & - \int_T^{T_i^{\mathrm{fus}}} \frac{\Delta c_{p,\,i}(T',P)}{T'}\, dT', \end{aligned} \tag{15}$$

where $\Delta c_{p,i}(T,P) = c_{p,i}^{\mathrm{L}}(T,P) - c_{p,i}^{\mathrm{S}}(T,P)$ is the difference between the heat capacity of the liquid phase $c_{p,i}^{\mathrm{L}}(T,P)$ and the heat capacity of the solid phase $c_{p,i}^{\mathrm{S}}(T,P)$. The equality $\Delta h_i^{\mathrm{fus}}(T_i^{\mathrm{fus}},P) = T_i^{\mathrm{fus}}\Delta s_i^{\mathrm{fus}}(T_i^{\mathrm{fus}},P)$ at T_i^{fus} , leads to the expression [52]

$$\begin{aligned} \ln a_i^{\mathrm{sat}}(T,P,\boldsymbol{x}^{\mathrm{sat}}) = \quad & -\frac{\Delta h_i^{\mathrm{fus}}(T_i^{\mathrm{fus}},P)}{R}\left(\frac{1}{T} - \frac{1}{T_i^{\mathrm{fus}}}\right) \\ & + \frac{1}{RT}\int_T^{T_i^{\mathrm{fus}}} \Delta c_{p,\,i}(T',P)\, dT' \\ & - \frac{1}{R}\int_T^{T_i^{\mathrm{fus}}} \frac{\Delta c_{p,\,i}(T',P)}{T'}\, dT'. \end{aligned} \tag{16}$$

If the heat capacity difference is only known at T_i^{fus}, the (reasonable) approximation $\Delta c_{p,\,i}(T,P) \approx \Delta c_{p,\,i}(T_i^{\mathrm{fus}},P)$ simplifies Eq. 16 to

$$\begin{aligned} \ln a_i^{\mathrm{sat}}(T,P,\boldsymbol{x}^{\mathrm{sat}}) = \quad & -\frac{\Delta h_i^{\mathrm{fus}}(T_i^{\mathrm{fus}},P)}{R}\left(\frac{1}{T} - \frac{1}{T_i^{\mathrm{fus}}}\right) \\ & - \frac{\Delta c_{p,\,i}(T_i^{\mathrm{fus}},P)}{R}\left(\ln\left(\frac{T_i^{\mathrm{fus}}}{T}\right) - \frac{T_i^{\mathrm{fus}}}{T} + 1\right). \end{aligned} \tag{17}$$

Although neglecting $\Delta c_{p,i}(T_i^{\mathrm{fus}},P)$ can affect significantly the solubility prediction [53, 49, 54], depending on the mixture and the temperature, experimental

values of $\Delta c_{p,i}(T_i^{\rm fus}, P)$ are unknown for most of the molecules considered in our work (an important exception is benzoic aicd). We hence do not take into account this term in our current calculations. Furthermore, as the SAFT-γ Mie approach relies on the characterisation of group parameters, which are used in a transferable manner, we choose to systematically neglect $\Delta c_{p,i}(T_i^{\rm fus}, P)$ in order to employ a consistent methodology for all groups and mixtures. Thus, Eq. 17 reduces to

$$\ln a_i^{\rm sat}(T, P, \boldsymbol{x}^{\rm sat}) = -\frac{\Delta h_i^{\rm fus}(T_i^{\rm fus}, P)}{R}\left(\frac{1}{T} - \frac{1}{T_i^{\rm fus}}\right). \tag{18}$$

A refinement of the models developed in our current work would be possible when values of the heat capacity difference become available, for the family of alkylbenzoic acids, diphenylamine, and mefenamic acid. The enthalpy of fusion $\Delta h_i^{\rm fus}(T_i^{\rm fus}, P_{\rm amb})$ and melting temperature $T_i^{\rm fus}$ of benzoic acid, diphenylamine, and mefenamic acid, are summarised in Table 2, and are used to determine the activity $a_i^{\rm sat}(T, P, \boldsymbol{x}^{\rm sat})$ and the solubility of these molecules in pure or mixed solvents.

Table 2: Average fusion enthalpy $\Delta h_i^{\rm fus}$ and fusion temperature $T_i^{\rm fus}$ of benzoic acid, diphenylamine, and mefenamic acid used in Eq. 18, for the calculation of the experimental activity coefficients and in all the SAFT-γ Mie calculations and predictions.

Compound i	$\Delta h_i^{\rm fus}(T_i^{\rm fus}, P_{\rm amb})$ / (kJ/mol)	$T_i^{\rm fus}$ / K	Ref.
Benzoic acid	17.909	395.64	[55, 56, 57, 58, 59, 60, 61] and current work
Diphenylamine	18.303	326.18	[62, 63, 64, 65, 66, 67, 68] and current work
Mefenamic acid	38.7	503.5	[66]

The activity a_i is related to the solute mole fraction and the activity coefficient by $a_i = x_i\gamma_i$, so that the solubility of i can be obtained as,

$$\ln x_i^{\rm sat}(T, P, \boldsymbol{x}^{\rm sat}) = -\frac{\Delta h_i^{\rm fus}(T_i^{\rm fus}, P)}{R}\left(\frac{1}{T} - \frac{1}{T_i^{\rm fus}}\right) - \ln\gamma_i(T, P, \boldsymbol{x}^{\rm sat}). \tag{19}$$

2.4. Parameter estimation

The parameters characterising the groups are determined by minimisation of an objective function $f_{\rm obj}$ given by,

$$\min_{\Theta} f_{\rm obj} = \frac{1}{N^{\rm exp}} \sum_{s=1}^{N^S} \sum_{p=1}^{N_s^P} \sum_{i=1}^{N_{s,p}^D} w_{s,p,i} \left(\frac{X_{s,p,i}^{\rm exp} - X_{s,p,i}^{\rm calc}(\Theta)}{X_{s,p,i}^{\rm exp}} \right)^2 , \tag{20}$$

where Θ is the vector of model parameters, $N^{\rm exp}$ is the total number of experimental points considered in the parameter estimation, N^S is the number of systems (pure compounds / mixtures) used in the estimation, N_s^P is the number of property types for system s, $N_{s,p}^D$ is the number of experimental data for system s and property p, $w_{s,p,i}$ is a weight that controls the relative importance of data point i for property p of system s. We consider here the same weight for each point (i.e., $w_{s,p,i} = 1$, for all points). $X_{s,p,i}^{\rm exp}$ is the $i^{\rm th}$ measured value of property p of system s, and $X_{s,p,i}^{\rm calc}(\Theta)$ is the corresponding value calculated with SAFT-γ Mie and the parameters Θ.

The percentage absolute average deviation (%AAD) of a property p for a system s,

$$\%{\rm AAD}_s[p] = \frac{1}{N_{s,p}^D} \sum_{i=1}^{N_{s,p}^D} \left| \frac{X_{s,p,i}^{\rm exp} - X_{s,p,i}^{\rm calc}}{X_{s,p,i}^{\rm exp}} \right| \times 100, \tag{21}$$

and the absolute average deviation,

$${\rm AAD}_s[p] = \frac{1}{N_{s,p}^D} \sum_{i=1}^{N_{s,p}^D} \left| X_{s,p,i}^{\rm exp} - X_{s,p,i}^{\rm calc} \right| , \tag{22}$$

are used as measures of the accuracy of the theoretical approach.

3. Results and discussion

3.1. Experimental results

Melting temperature and melting enthalpy. The DSC results for benzoic acid (BA), diphenylamine (DPA), and mefenamic acid (MFA) are presented in Fig. 2. For each compound, a single endotherm is obtained. Onset melting temperatures of $T_{\rm BA}^{\rm fus} = 395.98 \pm 0.04$ K and $T_{\rm DPA}^{\rm fus} = 326.18 \pm 0.04$ K, are recorded

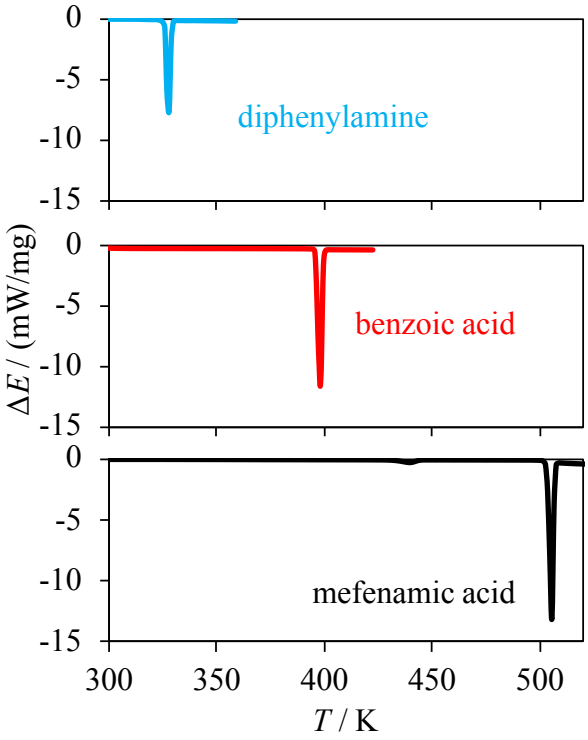

Figure 2: DSC analysis of diphenylamine (blue), benzoic acid (red), and mefenamic acid (black), with a heating rate of 10 K/min.

for benzoic acid and diphenylamine, respectively. The corresponding melting enthalpies are $\Delta h^{\mathrm{fus}}_{\mathrm{BA}} = 18.6 \pm 0.4$ kJ/mol and $\Delta h^{\mathrm{fus}}_{\mathrm{DPA}} = 15.8 \pm 0.5$ kJ/mol. As no phase transitions are detected before the onset of melting for each compound the melting enthalpy and melting temperature are those of the stable forms at room temperature.

The data of melting enthalpy found in recent literature for benzoic acid [55, 56, 57, 58, 59, 60, 61, 69] and diphenylamine [62, 63, 64, 65, 66, 67, 68] present a large dispersion of values, from 15 kJ/mol to 21 kJ/mol for these two molecules. For this reason, we employ here average values calculated from literature data with the addition of those measured in our current work (cf. Table 2). The average values are used both in the analysis of experimental data, and for the SAFT-γ Mie calculations and predictions.

In the case of mefenamic acid, a small endothermic signal can be seen at 433 K followed by a larger one at 501 K. During heating of this enantiotropic system, a solid-state transformation occurs from Form I, stable at room temperature, to Form II [5, 8, 10]. Therefore, the $\Delta h^{\mathrm{fus}}_{\mathrm{MFA}}$ and $T^{\mathrm{fus}}_{\mathrm{MFA}}$ for the stable polymorph used throughout this paper (Form I) could not be obtained. The melting enthalpy and melting temperature $T^{\mathrm{fus}}_{\mathrm{MFA}}$ corresponding to Form I and used in this work, are instead obtained from literature sources [66] (cf. Table 2).

Experimental solubilities. The measured solubilities are provided in the supplementary information (cf. Tables SI.1, SI.2, and SI.3), where the data can be found both in mole fraction, and grams per gram of solvent. The linear relationship

$$\ln x_i^{\mathrm{sat}} = \frac{\mathrm{A}_i}{T} + \mathrm{B}_i, \tag{23}$$

is often also used to present experimental data [47]. The curves in Fig. 3 are obtained using Eq. 23. The values for A_i (in K) and B_i corresponding to the measurements carried out in our work are provided in the supplementary information (cf. Table SI.4). The related van't Hoff plots for each compound in the respective solvent are also provided in the supplementary information (cf. Fig. SI.1).

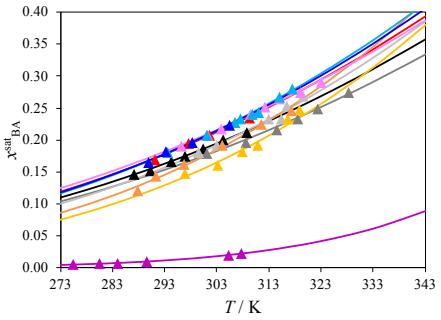

(a) Solubilities of benzoic acid

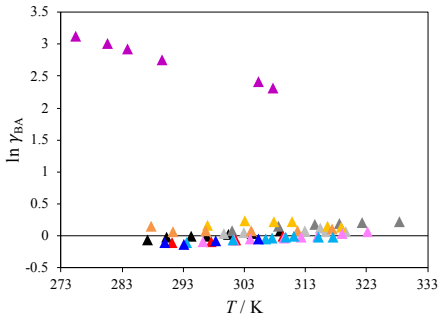

(b) Activity coefficients of benzoic acid

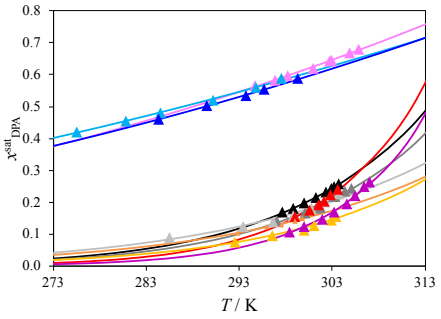

(c) Solubilities of diphenylamine

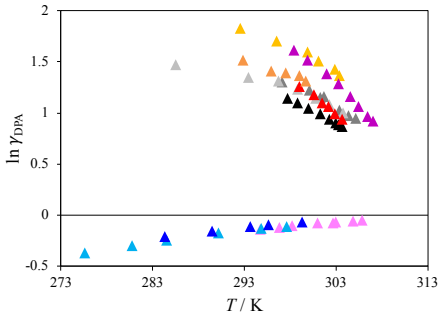

(d) Activity coefficients of diphenylamine

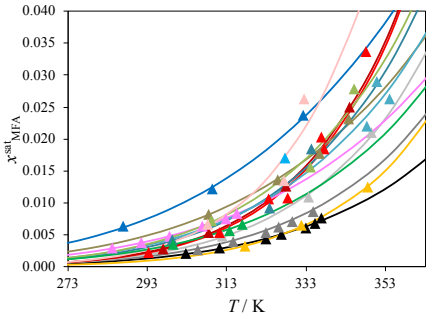

(e) Solubilities of mefenamic acid

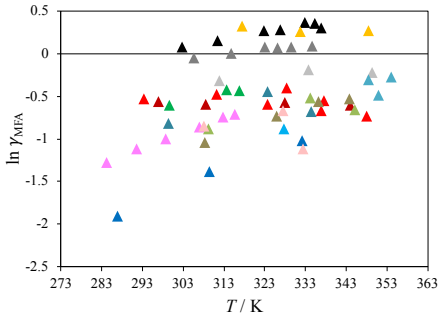

(f) Activity coefficients of mefenamic acid

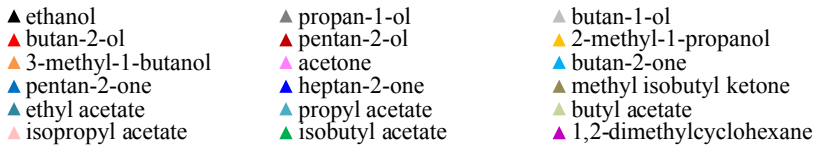

Figure 3: The symbols denote the experimental solubilities (left) and activity coefficients (right) of benzoic acid (a,b), diphenylamine (c,d), and mefenamic acid (e,f) in various solvents. The continuous curves are calculated using Eq.23. Experimental values and van't Hoff coefficients are provided in the supplementary information (cf. Tables SI.1, SI.2, and SI.3).

The solubility for benzoic acid in each solvent (Fig. 3(a)) at 303 K is presented from highest to lowest, following: acetone > heptan-2-one > butan-2-one > butan-2-ol > ethanol > butan-1-ol > 3-methyl-1-butanol > propanol > 2-methyl-1-propanol > 1,2-dimethylcyclohexane. Benzoic acid is significantly less soluble in 1,2-dimethylcyclohexane than in the other solvents, at only $x_{\mathrm{BA}}^{\mathrm{sat}} = 0.018$ at 303 K. The solubility in the remaining solvents ranges from $x_{\mathrm{BA}}^{\mathrm{sat}} = 0.16$ to 0.22. The highest solubilities of benzoic acid at 303 K are for the ketones, i.e., acetone, heptan-2-one, and butan-2-one, which present a similar solubility of $x_{\mathrm{BA}}^{\mathrm{sat}} \approx 0.20$.

For diphenylamine, the order of solubility at 303 K is: acetone > butan-2-one > heptan-2-one > ethanol > butan-2-ol > propanol > butan-1-ol > 3-methyl-1-butanol > 1,2-dimethylcyclohexane > 2-methyl-1-propanol (cf. Fig. 3(c)). The highest solubility $x_{\mathrm{DPA}}^{\mathrm{sat}} = 0.65$ is measured in acetone, followed by that in fellow ketones, with $x_{\mathrm{DPA}}^{\mathrm{sat}} = 0.63$ and $x_{\mathrm{DPA}}^{\mathrm{sat}} = 0.62$, in of butan-2-one and heptan-2-one, respectively. The lowest solubility $x_{\mathrm{BA}}^{\mathrm{sat}} = 0.15$ is measured in 2-methyl-1-propanol, closely followed by those in 1,2-dimethylcyclohexanol and 3-methyl-1-butanol (both with $x_{\mathrm{DPA}}^{\mathrm{sat}} \approx 0.17$). With respect to the alcohol family, the highest solubility is measured in ethanol, ($x_{\mathrm{DPA}}^{\mathrm{sat}} = 0.25$), followed by butan-2-ol $x_{\mathrm{DPA}}^{\mathrm{sat}} = 0.22$. (All of these correspond to values at 303 K.)

In the case of mefenamic acid, the solubility is found to be noticeably lower in all solvents considered. All of the measured solubilities, over temperature range considered, for all of the solvents, are below $x_{\mathrm{MA}} = 0.035$ (Fig. 3(e)). The order of solubility at 303 K is: pentan-2-one > methyl isobutyl ketone > acetone > butyl acetate > propyl acetate > isopropyl acetate > ethyl acetate > pentan-2-ol > isobutyl acetate > butan-2-ol > butan-1-ol > propan-1-ol > ethanol > 2-methyl-1-propanol. As with diphenylamine, and to a lesser extent benzoic acid, mefenamic acid has the largest measured solubility in solvents containing a ketone group, with mefenamic acid in pentan-2-one exhibiting the largest solubility at 303 K of $x_{\mathrm{MFA}}^{\mathrm{sat}} = 0.01$, followed by methyl isobutyl ketone and acetone ($x_{\mathrm{MFA}}^{\mathrm{sat}} = 0.0068$ and $x_{\mathrm{MFA}}^{\mathrm{sat}} = 0.0055$, respectively, at the same temperature). In the family of alcohol solvents, the highest measured soubility

is measured in pentan-2-ol ($x^{\text{sat}}_{\text{MFA}} = 0.0039$), and the lowest in 2-methyl-1-propanol ($x^{\text{sat}}_{\text{MFA}} = 0.0016$).

Summing up, considering the three compounds of interest in our current work, mefenamic acid presents the lowest solubility in comparison to benzoic acid and diphenylamine. The highest solubilities are measured in solvents containing ketone functional groups for all compounds considered, followed by the alcohols. As shown through the order of these solubilities at 303 K, the chain length within each solvent group further dictates the specific effectiveness of the solvent.

Activity coefficients. Through the determination of the activity coefficients for the measured solubility of each compound + solvent sample, a measure of the non-ideality of the solution can be gleaned. The activity coefficients γ_i for each compound i in its respective solvent can be calculated from the measured solubility using Eq. 19 and the data provided in Table 2. These values are plotted alongside the experimental solubilities in Fig. 3, and the data can be found in the supplementary information (cf. Tables SI.1, SI.2, and SI.3). As can be seen in the figure, the majority of the calculated activity coefficients of benzoic acid γ_{BA} are found to be close to 1 ($\ln \gamma_{\text{BA}}$ close to 0), indicating small deviations from ideal solution behaviour. A noticeable exception are the large values obtained in 1,2-dimethylcyclohexane. In the case of diphenylamine clear positive deviations are seen, with $\ln \gamma_{\text{DPA}} > 0$ for all solvents except the ketones, which are very good solvents for diphenylamine. For mefenamic acid, the lower solubility leads to more scatter in the calculated activity coefficients. It can be seen that most of the values of $\ln \gamma_{\text{MFA}} < 0$ for the MFA solutions, with only three of the solvents leading to positive values of $\ln \gamma_{\text{MFA}}$.

3.2. SAFT-γ Mie modelling

As seen in the previous section, the list of solvents considered in our work includes linear/branched alkanes, cyclohexane, benzene, acetates, 2-ketones, acetone, glycols, methanol and alcohols. The three solutes and each of these

solvents are decomposed into their SAFT-γ Mie functional groups, since, as described in Section 2.2, each individual group and group-group interaction contribute to the overall thermophysical properties of a system. Moreover, in the SAFT-γ Mie approach, the contribution of each functional group is considered to be independent of its position within the molecule, and the group-group interactions are transferable across systems.

Mefenamic acid (Fig. 1(a)) is modelled with seven aCH groups, two aCCH3 groups, one aCNHaC group and one aCCOOH group. Both the aCH and the $aCCH_3$ groups have been characterised previously [70, 50] while the models for the aCCOOH and aCCOOH groups are developed in our current work. Benzoic acid includes five aCH groups and one aCCOOH group, and diphenylamine with ten aCH groups and one aCNHaC group. In order to model the three compounds and their mixtures with the solvents of the list, the needed groups are identified, and are presented in Table 3. The parameters needed for the study are highlighted in green if estimated in this work, in blue if published already and marked with CR if combining rules are used.

Both the aCCOOH and aCNHaC groups contain aromatic carbons. In SAFT-γ Mie the group aCH is modelled with an associating site of type e to account for the delocalised electrons in the aromatic ring interacting with protic solvents (e.g., water). However neither of the models for the new groups developed in our current work carry this particular association site for different reasons. In the case of the aCCOOH group, four e-type association sites are incorporated to account for oxygen lone pairs, and one H site is incorporated corresponding to the hydrogen atom. It was found that a model for this group with these five association sites led to a better performance that a model with an additional "aromatic" e-site. In the case of the aCNHaC group, a good description of the thermodynamic properties of the systems evaluated is obtained with a model including one e site (corresponding to the nitrogen atom) and one H site (corresponding to the hydrogen atom).

The relevant like, unlike and association parameters are presented in Tables 4, 5, and 6. These tables include parameters previously presented [41, 45,

Table 3: Group and group-group parameters used to model mefenamic acid in a range of solvents using the SAFT-γ Mie approach.

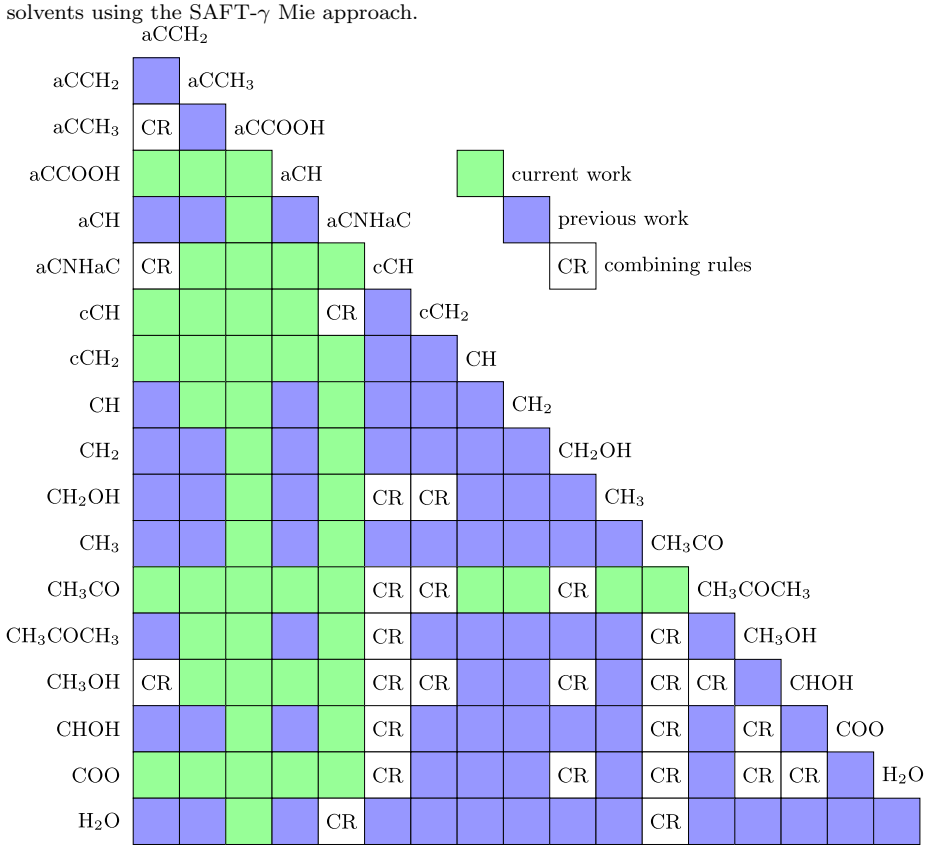

Table 4: SAFT-γ Mie group like parameters of the groups considered in our current work (excluding association). The asterisk symbol ($*$) indicates that the parameters are developed in our current work.

k	group	ν_k^*	S_k	σ_{kk} / Å	λ_{kk}^r	λ_{kk}^a	(ε_{kk}/k_B) / K	$N_{ST,k}$	$n_{k,H}$	n_{k,e_1}	n_{k,e_2}	Ref.
1	$aCCH_2$	1	0.20859	5.2648	8.5433	6	591.56	1	-	1	-	[50]
2	$aCCH_3$	1	0.31655	5.4874	23.627	6	651.41	1	-	1	-	[70]
3	aCCOOH	2	0.6553	3.3942	8.0000	6	313.35	3	1	2	2	*
4	aCH	1	0.32184	4.0578	14.756	6	371.53	1	-	1	-	[50]
5	aCNHaC	1	0.54263	3.3218	8.2761	6	303.35	3	1	1	-	*
6	cCH	1	0.0961	5.4116	8.0000	6	699.92	-	-	-	-	[43]
7	cCH_2	1	0.24751	4.7852	20.386	6	477.36	-	-	-	-	[50]
8	CH	1	0.0721	5.295	8.0000	6	95.621	-	-	-	-	[50]
9	CH_2	1	0.22932	4.8801	19.871	6	473.39	-	-	-	-	[41]
10	CH_2OH	2	0.58538	3.4054	22.699	6	407.22	2	1	2	-	[45]
11	CH_3	1	0.57255	4.0773	15.05	6	256.77	-	-	-	-	[41]
12	CH_3CO	2	0.54685	3.9112	19.05	6	525.22	1	-	2	-	*
13	CH_3COCH_3	3	0.72135	3.5981	17.433	6	286.02	3	1	1	1	[50]
14	CH_3OH	2	0.83517	3.2462	19.235	6	307.69	2	1	2	-	[50]
15	CHOH	2	0.18963	4.5381	18.185	6	599.66	2	1	2	-	[43]
16	COO	1	0.65264	3.9939	31.189	6	868.92	1	-	2	-	[41]
17	H_2O	1	1.00000	3.0063	17.020	6	266.68	2	2	2	-	[50, 42]

50, 70, 43, 71] and from our current work, estimated using the objective function given in Eq. 20. Pure compound vapour pressure, enthalpy of vapourisation, and saturated-liquid data, as well as mixture bubble pressure, bubble and dew temperature data are used in the refinement of the parameters that characterise the group-group interactions. Solubility data are used in parameter estimation only if no data for other property are available. However, since the simplest molecules containing the new groups aCCOOH and aCNHaC, i.e., benzoic acid and diphenylamine, are relatively heavy molecules, the data most available and therefore most used in the estimations of this work are solubility measurements.

Table 5: Unlike group parameters (excluding association) for use with the SAFT-γ Mie approach. The asterisk symbol ($*$) indicates that the parameters have been developed in our current work.

k	l	group k	group l	$(\varepsilon_{kl}/k_{\mathrm{B}})$ / K	λ^r_{kl}	Ref.
1	2	aCCH$_2$	aCCH$_3$	CR	CR	—
1	3	aCCH$_2$	aCCOOH	168.69	CR	$*$
1	4	aCCH$_2$	aCH	416.69	CR	[50]
1	5	aCCH$_2$	aCNHaC	CR	CR	—
1	6	aCCH$_2$	cCH	162.65	CR	$*$
1	7	aCCH$_2$	cCH$_2$	439.78	9.9058	$*$
1	8	aCCH$_2$	CH	65.410	CR	[50]
1	9	aCCH$_2$	CH$_2$	454.16	CR	[50]
1	10	aCCH$_2$	CH$_2$OH	434.37	CR	[71]
1	11	aCCH$_2$	CH$_3$	396.91	CR	[50]
1	12	aCCH$_2$	CH$_3$CO	663.71	30.712	$*$
1	13	aCCH$_2$	CH$_3$COCH$_3$	394.83	CR	[50]
1	14	aCCH$_2$	CH$_3$OH	CR	CR	—
1	15	aCCH$_2$	CHOH	357.91	CR	[43]
1	16	aCCH$_2$	COO	265.62	9.3393	$*$
1	17	aCCH$_2$	H$_2$O	329.03	CR	[71]
2	3	aCCH$_3$	aCCOOH	455.68	CR	$*$
2	4	aCCH$_3$	aCH	471.23	CR	[70]
2	5	aCCH$_3$	aCNHaC	941.03	CR	$*$
2	6	aCCH$_3$	cCH	792.29	CR	$*$
2	7	aCCH$_3$	cCH$_2$	540.63	21.082	$*$
2	8	aCCH$_3$	CH	769.36	8.0000	$*$
2	9	aCCH$_3$	CH$_2$	569.18	CR	[45]
2	10	aCCH$_3$	CH$_2$OH	486.62	CR	[71]
2	11	aCCH$_3$	CH$_3$	358.58	CR	[45]

k	l	group k	group l	$(\varepsilon_{kl}/k_{\mathrm{B}})$ / K	λ^r_{kl}	Ref.
2	12	aCCH$_3$	CH$_3$CO	552.62	36.429	$*$
2	13	aCCH$_3$	CH$_3$COCH$_3$	479.55	35.957	$*$
2	14	aCCH$_3$	CH$_3$OH	405.45	CR	$*$
2	15	aCCH$_3$	CHOH	762.86	CR	[43]
2	16	aCCH$_3$	COO	595.48	15.874	$*$
2	17	aCCH$_3$	H$_2$O	360.70	CR	[71]
3	4	aCCOOH	aCH	340.70	CR	$*$
3	5	aCCOOH	aCNHaC	102.98	CR	$*$
3	6	aCCOOH	cCH	246.61	CR	$*$
3	7	aCCOOH	cCH$_2$	389.90	CR	$*$
3	8	aCCOOH	CH	0.0000	CR	$*$
3	9	aCCOOH	CH$_2$	323.72	CR	$*$
3	10	aCCOOH	CH$_2$OH	172.57	9.2665	$*$
3	11	aCCOOH	CH$_3$	370.75	CR	$*$
3	12	aCCOOH	CH$_3$CO	568.75	85.000	$*$
3	13	aCCOOH	CH$_3$COCH$_3$	316.60	CR	$*$
3	14	aCCOOH	CH$_3$OH	290.16	8.0000	$*$
3	15	aCCOOH	CHOH	81.542	79.266	$*$
3	16	aCCOOH	COO	331.78	CR	$*$
3	17	aCCOOH	H$_2$O	228.58	9.5614	$*$
4	5	aCH	aCNHaC	549.72	CR	$*$
4	6	aCH	cCH	377.21	CR	$*$
4	7	aCH	cCH$_2$	393.05	15.377	$*$
4	8	aCH	CH	441.43	CR	[50]
4	9	aCH	CH$_2$	415.64	CR	[50]
4	10	aCH	CH$_2$OH	386.05	CR	[71]
4	11	aCH	CH$_3$	305.81	CR	[50]
4	12	aCH	CH$_3$CO	426.72	18.03	$*$
4	13	aCH	CH$_3$COCH$_3$	333.11	CR	[50]

k	l	group k	group l	$(\varepsilon_{kl}/k_{\mathrm{B}})$ / K	λ^r_{kl}	Ref.
4	14	aCH	CH_3OH	330.19	CR	$*$
4	15	aCH	CHOH	512.16	CR	[43]
4	16	aCH	COO	534.18	22.088	$*$
4	17	aCH	H_2O	357.78	38.640	[50]
5	6	aCNHaC	cCH	CR	CR	—
5	7	aCNHaC	cCH_2	564.85	CR	$*$
5	8	aCNHaC	CH	878.88	CR	$*$
5	9	aCNHaC	CH_2	347.75	CR	$*$
5	10	aCNHaC	CH_2OH	485.03	8.0012	$*$
5	11	aCNHaC	CH_3	647.64	CR	$*$
5	12	aCNHaC	CH_3CO	710.53	8.0000	$*$
5	13	aCNHaC	CH_3COCH_3	261.23	8.0000	$*$
5	14	aCNHaC	CH_3OH	398.10	CR	$*$
5	15	aCNHaC	CHOH	451.48	8.1810	$*$
5	16	aCNHaC	COO	809.96	CR	$*$
6	7	cCH	cCH_2	321.71	CR	[43]
6	8	cCH	CH	CR	CR	—
6	9	cCH	CH_2	522.57	CR	[43]
6	10	cCH	CH_2OH	CR	CR	—
6	11	cCH	CH_3	690.17	CR	[43]
6	12	cCH	CH_3CO	CR	CR	—
6	13	cCH	CH_3COCH_3	CR	CR	—
6	14	cCH	CH_3OH	CR	CR	—
6	15	cCH	CHOH	CR	CR	—
6	16	cCH	COO	CR	CR	—
6	17	cCH	H_2O	377.16	22.265	[72]
7	8	cCH_2	CH	570.45	CR	[50]
7	9	cCH_2	CH_2	469.67	CR	[50]
7	10	cCH_2	CH_2OH	CR	CR	—

k	l	group k	group l	$(\varepsilon_{kl}/k_{\mathrm{B}})$ / K	λ^r_{kl}	Ref.
7	11	cCH_2	CH_3	355.95	CR	[50]
7	12	cCH_2	CH_3CO	CR	CR	—
7	13	cCH_2	CH_3COCH_3	352.19	CR	[43]
7	14	cCH_2	CH_3OH	CR	CR	—
7	15	cCH_2	CHOH	554.50	CR	[43]
7	16	cCH_2	COO	498.60	CR	[50]
7	17	cCH_2	H_2O	350.99	28.000	[72]
8	9	CH	CH_2	506.21	CR	[50]
8	10	CH	CH_2OH	329.22	CR	[71]
8	11	CH	CH_3	387.48	CR	[50]
8	12	CH	CH_3CO	321.91	CR	∗
8	13	CH	CH_3COCH_3	637.29	CR	[50]
8	14	CH	CH_3OH	CR	CR	—
8	15	CH	CHOH	0.0000	CR	[43]
8	16	CH	COO	353.65	CR	[71]
8	17	CH	H_2O	275.75	CR	[71]
9	10	CH_2	CH_2OH	423.17	CR	[45]
9	11	CH_2	CH_3	350.77	CR	[41]
9	12	CH_2	CH_3CO	431.49	CR	∗
9	13	CH_2	CH_3COCH_3	299.48	11.594	[50]
9	14	CH_2	CH_3OH	341.41	17.05	[50]
9	15	CH_2	CHOH	517.64	CR	[43]
9	16	CH_2	COO	498.86	CR	[50]
9	17	CH_2	H_2O	423.63	100.00	[45]
10	11	CH_2OH	CH_3	333.20	CR	[45]
10	12	CH_2OH	CH_3CO	CR	CR	—
10	13	CH_2OH	CH_3COCH_3	338.47	CR	[43]
10	14	CH_2OH	CH_3OH	CR	CR	—
10	15	CH_2OH	CHOH	389.23	CR	[43]

k	l	group k	group l	$(\varepsilon_{kl}/k_{\mathrm{B}})$ / K	λ^r_{kl}	Ref.
10	16	CH_2OH	COO	CR	CR	—
10	17	CH_2OH	H_2O	353.37	CR	[45]
11	12	CH_3	CH_3CO	344.57	CR	∗
11	13	CH_3	CH_3COCH_3	233.48	14.449	[50]
11	14	CH_3	CH_3OH	275.76	15.537	[50]
11	15	CH_3	CHOH	479.38	CR	[43]
11	16	CH_3	COO	402.75	CR	[50]
11	17	CH_3	H_2O	358.18	100.00	[45]
12	13	CH_3CO	CH_3COCH_3	CR	CR	—
12	14	CH_3CO	CH_3OH	CR	CR	—
12	15	CH_3CO	CHOH	CR	CR	—
12	16	CH_3CO	COO	CR	CR	—
12	17	CH_3CO	H_2O	CR	CR	—
13	14	CH_3COCH_3	CH_3OH	CR	CR	—
13	15	CH_3COCH_3	CHOH	340.81	CR	[43]
13	16	CH_3COCH_3	COO	547.44	CR	[43]
13	17	CH_3COCH_3	H_2O	287.26	CR	[50]
14	15	CH_3OH	CHOH	CR	CR	—
14	16	CH_3OH	COO	CR	CR	—
14	17	CH_3OH	H_2O	278.45	CR	[50]
15	16	CHOH	COO	CR	CR	—
15	17	CHOH	H_2O	479.16	CR	[43]
16	17	COO	H_2O	396.81	15.140	[43]

Table 6: Group association parameters for use with the SAFT-γ Mie approach. The asterisk symbol ($*$) indicates that the parameters have been developed in our current work.

k	l	group k	site a of group k	group l	site b of group l	$(\varepsilon_{kl}^{\mathrm{HB}}/k_{\mathrm{B}})$ / K	$K_{kl,ab}$ / Å^3	Ref.
1	3	$aCCH_2$	e	aCCOOH	H	3961.5	0.023401	$*$
1	17	$aCCH_2$	e	H_2O	H	563.56	339.61	[71]
2	3	$aCCH_3$	e	aCCOOH	H	3961.5	0.023401	$*$
2	17	$aCCH_3$	e	H_2O	H	563.56	339.61	[71]
3	3	aCCOOH	H	aCCOOH	H	4745.7	10.04	$*$
3	4	aCCOOH	H	aCH	e	3961.5	0.023401	$*$
3	5	aCCOOH	H	aCNHaC	e	2424.1	990.46	$*$
3	10	aCCOOH	e_1	CH_2OH	H	1284.9	2978.8	$*$
3	10	aCCOOH	e_2	CH_2OH	H	3889.3	0.43712	$*$
3	10	aCCOOH	H	CH_2OH	e	1284.9	2978.8	$*$
3	12	aCCOOH	H	CH_3CO	e	2828.1	47.677	$*$
3	13	aCCOOH	H	CH_3COCH_3	e_1	2732.9	478.38	$*$
3	14	aCCOOH	e_1	CH_3OH	H	1400.7	495.32	$*$
3	14	aCCOOH	H	CH_3OH	e	871.46	0.25605	$*$
3	15	aCCOOH	e_1	CHOH	H	2278.5	73.698	$*$
3	15	aCCOOH	e_2	CHOH	H	2278.5	73.698	$*$
3	15	aCCOOH	H	CHOH	e	2278.5	73.698	$*$
3	16	aCCOOH	H	COO	e	1772.3	945.09	$*$
3	17	aCCOOH	e_1	H_2O	H	882.05	984.34	$*$
3	17	aCCOOH	e_2	H_2O	H	882.05	984.34	$*$
3	17	aCCOOH	H	H_2O	e	5192.5	0.011186	$*$
4	17	aCH	e	H_2O	H	563.56	339.61	[50]
5	13	aCNHaC	H	CH_3COCH_3	e_1	2208.9	750.72	$*$
5	14	aCNHaC	e	CH_3OH	H	2346.0	3.1536	$*$

k	l	group k	site a of group k	group l	site b of group l	$(\varepsilon_{kl}^{\mathrm{HB}}/k_{\mathrm{B}})$ / K	$K_{kl,ab}$ / Å^3	Ref.
5	14	aCNHaC	H	CH_3OH	e	2346.0	3.1536	$*$
10	10	CH_2OH	H	CH_2OH	e	2097.9	62.309	[45]
10	13	CH_2OH	e	CH_3COCH_3	H	686.93	585.99	[43]
10	13	CH_2OH	H	CH_3COCH_3	e_1	1844.8	991.95	[43]
10	15	CH_2OH	e	CHOH	H	1464.1	591.55	[43]
10	15	CH_2OH	H	CHOH	e	2500.0	10.444	[43]
10	17	CH_2OH	e	H_2O	H	621.68	425.00	[45]
10	17	CH_2OH	H	H_2O	e	2153.2	147.40	[45]
13	13	CH_3COCH_3	H	CH_3COCH_3	e_1	980.2	2865.2	[50]
13	15	CH_3COCH_3	e_1	CHOH	H	1323.1	635.37	[43]
13	15	CH_3COCH_3	H	CHOH	e	1186.9	731.08	[43]
13	17	CH_3COCH_3	e_1	H_2O	H	1588.7	772.77	[50]
13	17	CH_3COCH_3	e_2	H_2O	H	417.24	1304.3	[50]
13	17	CH_3COCH_3	H	H_2O	e_1	1386.8	188.83	[50]
14	14	CH_3OH	H	CH_3OH	e	2062.1	106.57	[50]
14	17	CH_3OH	e	H_2O	H	1993.5	104.11	[50]
14	17	CH_3OH	H	H_2O	e	1993.5	104.11	[50]
15	15	CHOH	H	CHOH	e	2480.6	8.474	[43]
15	17	CHOH	e_1	H_2O	H	2140.9	19.478	[43]
15	17	CHOH	H	H_2O	e_1	2289.1	63.813	[43]
16	17	COO	e	H_2O	H	1245.8	454.98	[43]
17	17	H_2O	H	H_2O	e	1985.4	101.69	[50, 42]

The parameter estimation is carried out in a successive manner, such that new groups are characterised based on previously determined group parameters. In view of the large number of groups developed in our current work (see green squares in Table 3), it is not practical to describe comprehensively the performance of the SAFT-γ Mie model in the prediction of the full range of thermodynamic properties of the very many molecules that can be modelled

using the new groups. Accordingly, we proceed to analyse first the performance of the aCCOOH group in predicting the properties of selected compounds and mixtures containing this group, as well as benzoic acid solubilities. We carry out a similar study of the aCNHaC group model, together with diphenylamine solubilities, and finish the Results section presenting mefenamic acid solubilities; these rely on (and confirm) the quality of the aCCOOH and aCNHaC models developed.

3.3. Benzoic acid

The group interaction parameters required to model benzoic acid, represented (Fig. 1(b)), and its interactions with other compounds are estimated using experimental phase equilibrium data of pure compounds (e.g., benzoic acid and methylbenzoic acids) and binary mixtures (e.g., benzoic acid + benzene). NIST data [73] are used for the pure compounds and data found in references [74, 75, 76, 77, 78, 79, 80, 81, 82] are used for the mixtures. These data are used to estimate simultaneously the aCCOOH-aCCOOH like group interaction parameters and the unlike interaction parameters between the aCCOOH group and groups $aCCH_2$, $aCCH_3$, aCH, CH_2, and CH_3. All the relevant experimental data used in the parameter estimation for these interactions are cited in Tables 7 and 8 together with the corresponding deviations obtained with SAFT-γ Mie calculations.

Overall, the parameters estimated offer a satisfactory description of the pure-compound data, with %AADs for the vapour pressure, saturated densities, vapourisation enthalpies and densities typically below 5% (up to 10% for the 3-ethylbenzoic acid). The AADs follow generally the same trend of the %AADs with the exception of benzoic acid, for which the experimental data are reported with a large uncertainty (see Fig. 4(a)), preventing a proper analysis. In the SAFT-γ Mie approach, isomers that share the same functional groups are non-distinguishable. This means that it is not possible to describe with SAFT-γ Mie differences in properties between isomers, and trade-offs take place. Resulting from this trade-off, the saturated densities for 4-methylbenzoic acid are

Table 7: Overview of accuracy of SAFT-γ Mie in the calculation of vapour pressures, saturated densities, vapourisation enthalpies and densities for pure compounds containing aCCOOH. All the data displayed are generated by NIST [73] and have been used in the parameter estimation procedure. $N^D_{s,p}$ is the number of experimental data for system s and property p.

Compound s	T range / K	$N^D_{s,p}$	%AAD$_s$ $P_{\text{vap}}(T)$	AAD$_s$ P_{vap} / Pa	Ref.
benzoic acid	425-545	25	0.983	522.4	[73]
2-ethylbenzoic acid	338-355	5	8.115	1.30	[73]
Compound s	T range / K	$N^D_{s,p}$	%AAD$_s$ $\rho_{\text{sat,liq}}(T)$	AAD$_s$ $\rho_{\text{sat,liq}}$ / (kg/m^3)	Ref.
benzoic acid	395-670	37	1.272	0.735	[73]
2-methylbenzoic acid	510-630	13	7.178	67.67	[73]
3-methylbenzoic acid	570-630	7	7.124	64.18	[73]
4-methylbenzoic acid	453-700	26	1.077	8.52	[73]
3-ethylbenzoic acid	530-590	7	9.729	92.74	[73]
4-ethylbenzoic acid	384-680	31	2.205	18.52	[73]
3-propylbenzoic acid	400-650	27	4.779	41.99	[73]
4-propylbenzoic acid	460-700	25	1.587	11.73	[73]
Compound s	T range / K	$N^D_{s,p}$	%AAD$_s$ $h_{\text{vap}}(T)$	AAD$_s$ h_{vap} / (J/mol)	Ref.
2-ethylbenzoic acid	420-480	7	2.008	1332	[73]
3-ethylbenzoic acid	390-480	10	3.634	2640	[73]
Compound s	T range / K P range / MPa	$N^D_{s,p}$	%AAD$_s$ $\rho(T,P)$	AAD$_s$ ρ / (kg/mol)	Ref.
3-ethylbenzoic acid	600-680 0.200-0.446	12	3.341	0.341	[73]

better described than those for 2- and 3-methylbenzoic acids, and similarly, a better description is obtained for the saturated densities of 4-ethylbenxoic and 4-propylbenzoic acids (see Table 7).

The experimental mixture data used in the characterisation of the group interactions (see Table 8) have been extracted from a range of publications concerning dew and bubble temperature [74, 75], bubble pressure [76, 77] and solubility [78, 79, 80, 81, 82, 83, 84] data. The agreement between the calculations and the experiments, in terms of %AAD is typically lower than 8% for benzoic acid in benzene (5.0%), and water (4.5%); in the case of 3-methylbenzoic acid in hexane the %AAD = 5.0%; and for 4-methylbenzoic acid in water is 7.8%. , Larger deviations are noted for benzoic acid in methylbenzene (12.3%), pentane (16.5%), hexane (17.3%), and heptane (69.7%). The larger deviations observed

Table 8: Overview of accuracy of SAFT-γ Mie in the calculation of bubble temperatures T_{bub} and pressures P_{bub}, dew temperatures T_{dew} and solubilities x_{sat} for binary systems. All the data displayed have been used in the parameter estimation procedure.

System s (1+2)	P range / MPa	x_1 range	$N^D_{s,p}$	%AAD$_s$ T_{bub}	AAD$_s$ T_{bub} / K	Ref.
benzoic acid + methylbenzene	0.053-0.080	0.01-0.40	18	0.081	0.302	[74]
benzoic acid + dibenzyl	0.013-0.100	0.10-0.70	18	1.960	9.82	[75]
System s (1+2)	P range / MPa	x_1 range	$N^D_{s,p}$	%AAD$_s$ T_{dew}	AAD$_s$ T_{dew} / K	Ref.
benzoic acid + methylbenzene	0.053-0.080	0.00-0.01	18	2.709	10.08	[74]
System s (1+2)	T range / K	x_1 range	$N^D_{s,p}$	%AAD$_s$ P_{bub}	AAD$_s$ P_{bub} / Pa	Ref.
benzoic acid + benzene	413	0.04-1.00	13	3.460	6097	[77]
benzoic acid + methylbenzene	413-423	0.01-1.00	22	5.632	6190	[76, 77]
System s (1+2)	T range / K	P range / MPa	$N^D_{s,p}$	%AAD$_s$ x_2^{sat}	AAD$_s$ x_2^{sat}	Ref.
benzoic acid + benzene	277-278	0.101	3	4.990	0.002	[78]
benzoic acid + methylbenzene	273-383	0.101	13	12.26	0.019	[79]
benzoic acid + pentane	283-323	0.101	4	16.46	0.002	[80]
benzoic acid + hexane	312-362	0.101	15	17.28	0.012	[81]
benzoic acid + heptane	283-303	0.101	3	69.70	0.007	[80]
3-methylbenzoic acid + hexane	298	0.101	1	5.041	0.001	[82]
benzoic acid + water	298-368	0.101	17	4.460	0.0002	[83]
4-methylbenzoic acid + water	288-371	0.101	23	7.846	0.00002	[84]

for the solubility in some alkanes are in part due to the extremely low solubilities of these systems, such that larger uncertainties can be expected in the experimental data, as well as higher sensitivity to the group parameters. Further refinement of these models and the consideration of second-order functional groups will be subject of future work.

In Fig. 4, calculations with SAFT-γ against NIST correlated experimental data [73]: vapour pressures Fig. 4(a) and saturated densities Fig. 4(b) of benzoic acid. As can be seen in the Fig. 4, the calculations fall within the uncertainty limits of the data used in the development of model parameters. We note also the overprediction of the critical temperature in the phase diagram presented, this can be expected, as the SAFT-γ Mie equation of state does not incorporate critical fluctuations.

An overview of the predictive accuracy of the SAFT-γ Mie model in pre-

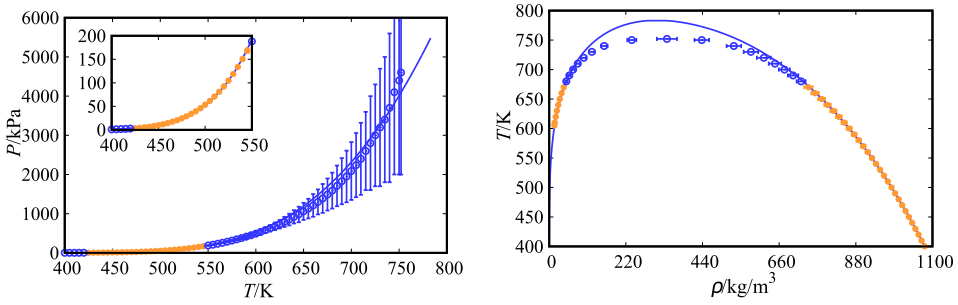

Figure 4: a) Vapour pressures for benzoic acid, b) saturated densities for benzoic acid. The curves represent SAFT-γ Mie calculations, the symbols represent NIST-generated data [73] that was used in the estimations (orange filled symbols) and not used (blue open symbols). The estimated error in the experimental data is shown with the error bars.

sented in Table 9 and Fig. 5. In Table 9, the predictive capability of SAFT-γ Mie for vapour pressures and saturated densities is tested for a range of pure compounds of the family of benzoic acid. In Fig. 5, the SAFT-γ Mie calculations are plotted against all solubility measurements found in literature for the systems of interest, in addition to the new data measured in our current work (see Sections 2.1 and 3.1).

In Table 9 the %AAD and ADD for the comparison of the SAFT-γ Mie calculations with saturation data for benzoic acid and eight other compounds of its family (at conditions between 30% and 90% of the critical temperature) are presented. Only a small fraction of the experimental data (those for which the reported relative uncertainty is lower than 5 %) are used in the development of the group interactions, meaning that the data presented in this table provides a good indication of the predictive accuracy of the approach. We note especially the good agreement of the SAFT-γ Mie model for benzoic acid for both the vapour pressure (%AAD = 5%) and the saturated liquid density (%AAD = 0.1%).

The methyl group of methylbenzoic acid can be positioned in the second, third, or fourth carbon of the aromatic ring. Although in the SAFT-γ Mie model it is not possible to differentiate these molecules with first-order groups as used

Table 9: Overview of accuracy of SAFT-γ Mie for the prediction of vapour pressures P_{vap} and saturated densities ρ_{sat} for a range of pure compounds of the family of benzoic acid. Only a small fraction of these data (those with smaller experimental uncertainty was used in the estimations.

Compound s	T range / K	$N^D_{s,p}$	%AAD$_s$ $P_{\text{vap}}(T)$	AAD$_s \times 10^{-3}$ P_{vap} / Pa	Ref.
benzoic acid	395-675	57	5.01	36	[73]
2-methylbenzoic acid	377-675	61	43.2	89	[73]
3-methylbenzoic acid	382-695	64	39.7	70	[73]
4-methylbenzoic acid	453-705	52	54.5	122	[73]
2-ethylbenzoic acid	338-680	70	4.13	3.7	[73]
3-ethylbenzoic acid	318-695	77	59.8	57	[73]
4-ethylbenzoic acid	385-710	67	26.5	84	[73]
3-propylbenzoic acid	316-690	76	13.2	16	[73]
4-propylbenzoic acid	422-705	58	31.7	82	[73]
Compound s	T range / K	$N^D_{s,p}$	%AAD$_s$ $\rho_{\text{sat,liq}}(T)$	AAD$_s$ $\rho_{\text{sat,liq}}$ / (kg/m^3)	Ref.
benzoic acid	395-670	29	0.068	0.58	[73]
2-methylbenzoic acid	377-670	31	12.4	123	[73]
3-methylbenzoic acid	382-690	32	12.3	118	[73]
4-methylbenzoic acid	453-700	26	7.27	62	[73]
2-ethylbenzoic acid	338-680	36	8.09	80	[73]
3-ethylbenzoic acid	318-690	39	9.84	98	[73]
4-ethylbenzoic acid	385-710	34	2.67	22	[73]
3-propylbenzoic acid	316-690	39	5.78	53	[73]
4-propylbenzoic acid	422-700	29	1.48	11	[73]

here, it is interesting, to assess the accuracy of the model for these isomers. The model developed captures best the vapour pressures of the 3-methylbenzoic acid (%AAD = 40%) and the liquid saturation densities of the 4-methylbenzoic acid (%AAD = 7%). The highest %AAD observed is 55% for the vapour pressures of 4-methylbenzoic acid. In relation to this error, is worth mentioning that the uncertainties reported in NIST for this compounds are also larger than for some of the other compounds [73].

Ethylbenzoic acid has also three position isomers, and it is encouraging to note that the deviations in the comparison of the SAFT-γ predictions and the experimental data are overall smaller for these molecules s compared to the

methyl substituted acid. The model captures best the vapour pressures of the 2-ethylbenzoic acid (%AAD = 4%) and the liquid saturation densities of the 4-ethylbenzoic acid (%AAD = 3%). The highest %AAD observed is 60% for the vapour pressures of 3-ethylbenzoic acid. Concerning the position isomers of propylbenzoic acid, the model captures best the vapour pressures of the 3-propylbenzoic acid (%AAD = 13%) and the liquid saturation densities of the 4-propylbenzoic acid (%AAD = 2%). The highest %AAD observed is 32% for the vapour pressures of 4-propylbenzoic acid. In future work it will be of interest to consider the incorporation of second-order groups to account for differences between isomers, in order to reduce these errors.

In terms of the performance of the SAFT-γ Mie approach for the calculation and prediction of solubility with the new group-interactions developed here, we present in Fig. 5 a parity plot comparing all the available experimental data for the solvents of interest. Experimental data form the literature as well as those those measured as part of our current work are included. The available experimental solubility data of benzoic acid are mostly limited to a small range of temperature, close to the ambient temperature. The data is often limited to a few points, which means that each point has a significant impact in the %ADD, and in addition, the solubilities can be very low in some of the solvents, leading to large %AADs. Thus, it is also useful to consider the absolute errors (AADs) and parity plots, to develop an overall assessment of the predictive accuracy of the model.

As can be seen in Fig. 5, the SAFT-γ Mie calculations fall within less than half an order of magnitude away from the measurements, which, within the context of predictive solubility methods, can be considered a satisfactory level of agreement. Moreover, we note that the agreement is seen to be best for the systems exhibiting higher solubility.

3.4. Diphenylamine

The like aCNHaC-aCNHaC and unlike interaction parameters aCNHaC-$aCCH_3$ and aCNHaC-aCH groups needed to model diphenylamine (Fig. 1(c)), as

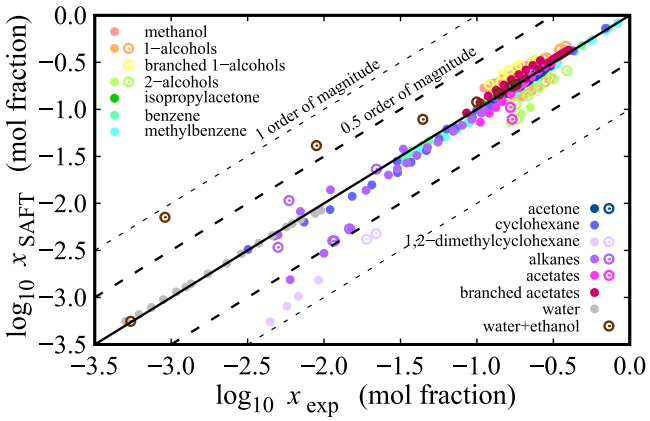

Figure 5: Solubility of benzoic acid calculated with SAFT-γ Mie vs experimental data. Data used for in the characterisation of group-interaction parameters are represented with filled symbols and those not used, with open symbols. Thermodynamic conditions are detailed in the supplementary information (cf. Table SI.5).

well as their interactions with other relevant groups, are estimated using experimental phase equilibrium data of pure diphenylamine, 3-methyldiphenylamine and dip-tolylamine [73], as well as mixture data of diphenylamine in benzene, methylbenzene, and 1,3-dimethylbenzene [85, 86, 87, 88, 89].

All the experimental data used in the parameter estimation are referenced in Tables 10 and 11, together with the corresponding model deviations. Overall, the SAFT-γ Mie approach using the parameters estimated provide a satisfactory description of the pure compound properties considered (Table 10), with %AADs for the vapour pressures and saturated densities typically below 5% (although we note the larger deviation of 13% in the case of 3-methyldiphenylamine).

In terms of the mixture data used (Table 11), these are obtained from publications concerning single phase densities [85, 86, 87, 88] and solid-liquid solubility [89]. The single-phase densities of the benzene + diphenylamine mixture are described with a %AAD of 2%, while in the case of the solid-liquid solubility calculations compared to the experimental data the %AAD is in the range 10% - 47%. The largest deviation is obtained for the case of diphenylamine in 1,3-dimethylbenzene. As we discussed in Section 3.3, it is not possible to

Table 10: Overview of accuracy of SAFT-γ Mie in the calculation of vapour pressures and saturated liquid densities for pure compounds containing the aCNHaC group. All the data displayed are obtained from NIST correlations [73] and are used in the parameter estimation procedure.

Compound s	T range / K	$N^D_{s,p}$	%AAD$_s$ $P_{\text{vap}}(T)$	AAD$_s$ $\times 10^{-3}$ P_{vap} / Pa	Ref.
diphenylamine	510-680	18	2.624	4.19	[73]
3-methyldiphenylamine	545-765	23	12.67	21.2	[73]
Compound s	T range / K	$N^D_{s,p}$	%AAD$_s$ $\rho_{\text{sat,liq}}(T)$	AAD$_s$ $\rho_{\text{sat,liq}}$ / (kg/m^3)	Ref.
diphenylamine	330-710	24	1.004	7.822	[73]
3-methyldiphenylamine	400-760	24	4.193	30.52	[73]
di-p-tolylamine	410-770	23	6.765	37.51	[73]

Table 11: Overview of accuracy of SAFT-γ Mie in the calculation of properties of binary mixtures of diphenylamine. Single-phase mixture density ρ (the mole fraction range considered is $x_{\text{DPA}} = [0.00 - 0.19]$) and solid-liquid solubility of diphenylamine $x^{\text{sat}}_{\text{DPA}}$, both at $P = 0.101$ MPa. All the data included are used in the parameter estimation procedure.

Solvent s	T range / K	$N^D_{s,p}$	%AAD$_s$ ρ	AAD$_s$ ρ / (kg/m^3)	Ref.
benzene	293-298	12	1.729	15.30	[85, 86, 87, 88]
Solvent s	T range / K	$N^D_{s,p}$	%AAD$_s$ $x^{\text{sat}}_{\text{DPA}}$	AAD$_s$ $x^{\text{sat}}_{\text{DPA}}$	Ref.
benzene	273-313	3	9.960	0.054	[89]
methylbenzene	273-313	3	19.21	0.096	[89]
1,3-dimethylbenzene	273-313	3	46.62	0.174	[89]

differentiate positional isomers with our current first-order groups. In future work, we will develop second order groups in order to improve the accuracy of the description of the properties in these systems.

In Fig. 6, SAFT-γ Mie calculations are shown against pseudo-experimental data [73] for the vapour pressures of diphenylamine, Fig. 6(a), the saturated densities of diphenylamine, Fig. 6(b), the saturated densities of 3-methyldiphenylamine, Fig. 6(c), and the heat capacities of diphenylamine, Fig. 6(d). The calculations presented in Fig. 6(d) are predictive, as no heat-capacity data is used for the characterisation of group interactions. The calculations are found to be in good agreement with the experimental data. In order to have an accurate description of pure diphenylamine properties, the accuracy on the saturated liquid

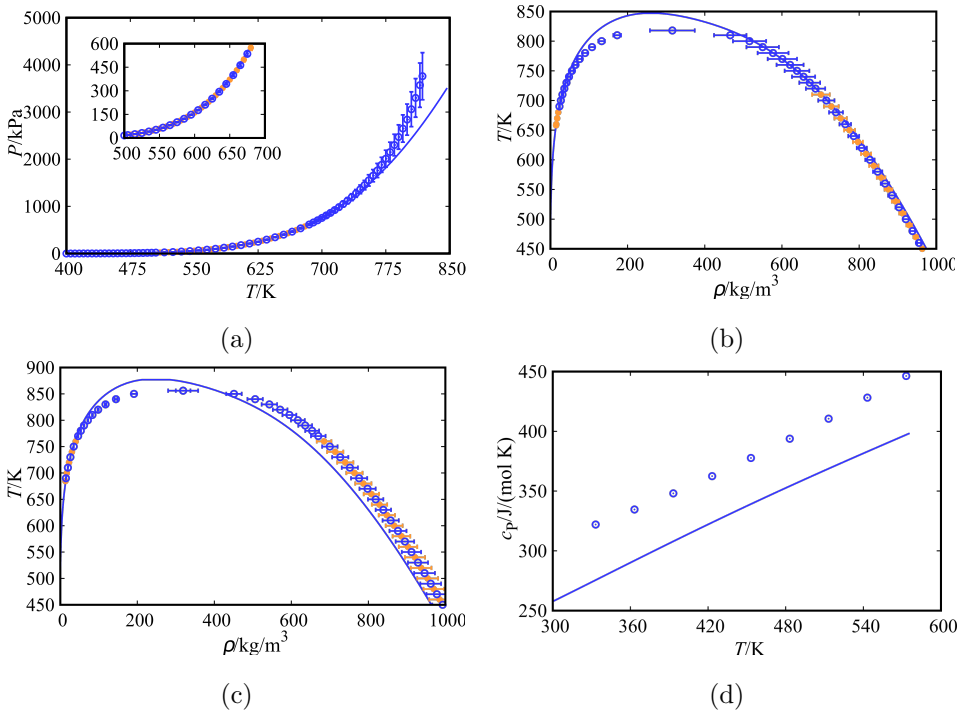

Figure 6: a) vapour pressures for diphenylamine, b) saturated densities for diphenylamine, c)saturated densities for 3-methyldiphenylamine and d) heat capacities for pure diphenylamine. The curves represent SAFT-γ Mie calculations, the symbols in a), b) and c) represent NIST-generated data [73] that was used in the estimations (orange filled symbols) and not (blue open symbols), and the symbols in d) represent experimental data [90]. The estimated error in the experimental data (when available) is shown with the error bars.

densities for 3-methyldiphenylamine was sacrificed slightly. This compromise could have potentially been avoided with a more sophisticated aCNHaC model, e.g. a model with an extra association site type – a study that was prevented due to the paucity of experimental data. The prediction of the heat capacities (Fig. 6 (d)), a second-derivative property, is achieved with great accuracy, which provides confidence to the model; especially accounting for the fact that this property was not included in the objective function used to carry out the model development.

Moreover, the prediction capability of SAFT-γ Mie of vapour pressures and saturated densities is tested for a range of pure compounds of the family of diphenylamine, and the calculated %AADs and AADs presented in Table 12. The data referenced in the table consists of vapour pressures and saturated densities for diphenylamine, 3,3'-dimethyldiphenylamine and di-p-tolylamine conditions between 30% and 90% of the critical temperature. Only a small fraction of these data (that including the points with the smallest uncertainty) was used in the estimations, which means that Table 12 provides a good indication of the quality of the parameters developed. The SAFT-γ Mie model for diphenylamine shows great performance across the whole range of temperatures for both vapour pressures (%AAD = 3.7%) and liquid saturated densities (%AAD = 1.0%).

Table 12: Overview of accuracy of SAFT-γ Mie in the calculation of vapour pressures and saturated densities for a range of pure compounds of the family of diphenylamine. Only a small fraction of these data was used in the estimations.

Compound s	T range / K	$N^D_{s,p}$	%AAD$_s$ $P_{\text{vap}}(T)$	AAD$_s \times 10^{-3}$ P_{vap} / Pa	Ref.
diphenylamine	326.32-735	83	3.69	3.3	[73]
3,3'-dimethyldiphenylamine	361.1-770	83	31.9	12	[73]
di-p-tolylamine	352.1-775	86	29	12	[73]
Compound s	T range / K	$N^D_{s,p}$	%AAD$_s$ $\rho_{\text{sat,liq}}(T)$	AAD$_s$ $\rho_{\text{sat,liq}}$ / (kg/m^3)	Ref.
diphenylamine	326.32-730	42	1.01	9.4	[73]
3,3'-dimethyldiphenylamine	361.1-770	42	4.21	36	[73]
di-p-tolylamine	352.1-770	43	5.02	44	[73]

Having assessed the performance of the models for the description and pre-

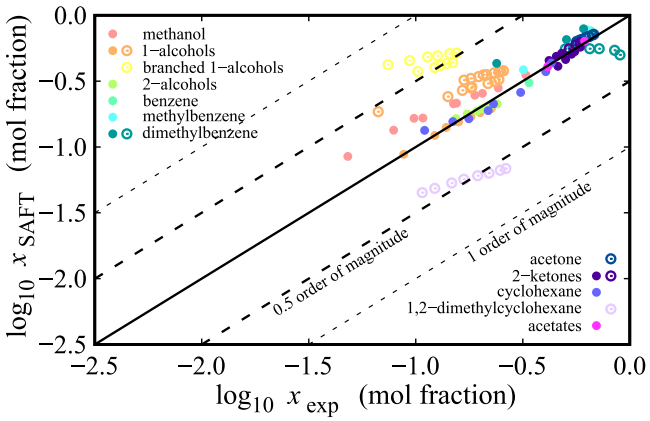

Figure 7: Solubility of diphenylamine calculated with SAFT-γ Mie against experimental measurements. Data used in the estimations are represented with filled symbols and those not used, with open symbols. Thermodynamic conditions are detailed in the supplementary information (cf. Table SI.6).

diction of fluid-phase equilibria, it is now of interest to consider the accuracy of the models for the description of the solid-liquid solubility of diphenylamine. In Fig. 7, the SAFT-γ Mie calculations are plotted against all solubility measurements for diphenylamine in a range of solvents, as found in the literature for the systems of interest, as well as those measured for this work (see Sections 2.1 and 3.1). As before, we report the SAFT-γ Mie calculations for solubility of diphenylamine in a parity plot for best comparison of all the data available. As can be seen in Fig. 7 our SAFT-γ calculations fall within an order of magnitude away from the measurements, with only limited scatter seen in the plot reduced scatter. The best agreement between the SAFT-γ calculations and the experimental data is seen for methanol, 2-butanol, acetone, benzene, methylbenzene, dimethylbenzene and hexane.

3.5. Mefenamic acid

The newly defined groups and the group-group interactions developed in the previous sections are now used to model the properties of systems containing mefenamic acid (Fig. 1(a)). In Fig. 8 an overview of the accuracy of the model is

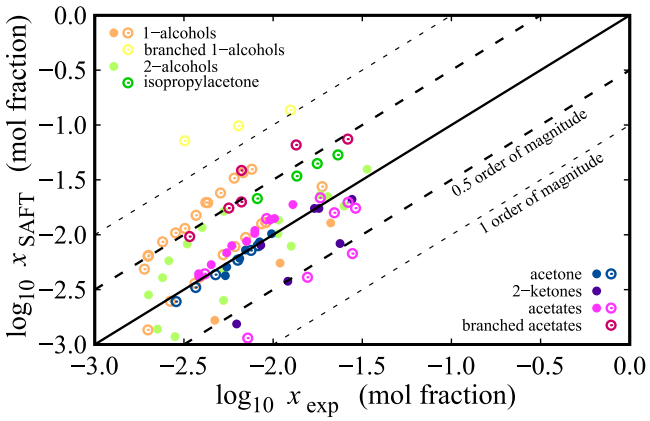

Figure 8: Solubility of mefenamic acid calculated with SAFT-γ Mie vs experimental measurements. Data used in the estimations are represented with filled symbols and those not used, with open symbols. Thermodynamic conditions are detailed in the supplementary information (cf. Table SI.7).

shown for all solubility data of mefenamic acid found in literature and measured in this work that can be currently modelled by SAFT-γ Mie. As can be gleaned, the scatter in the data is greater as compared to those for benzoic acid (Fig. 5) and diphenylamine (Fig. 7). This can be expected, as mefenamic acid is the most complex, of the tree molecules considerd, and the least soluble. Our SAFT-γ Mie model of mefenamic acid involves a larger set of group-group interactions, most of which have been refined using experimental properties related to benzoic acid and diphenylamine, meaning that a large part of the points presented correspond to predictions. Note in Fig. 8 that open symbols refer to predictive calculations. Despite the challenging nature of the molecule, the solubility calculations are within an order of magnitude of the experimental measurements, with the exception of the solubility in 2-methyl-1-propanol. We also note the excellent level of agreement obtained for the solubility of mefenamic acid in most acetates, 2-alcohols and acetone.

3.6. Solid-liquid solubility phase diagrams

We now present in more detail temperature-composition solubility phase diagrams for the three compounds of interest, in a selection of the solvents considered. All of the calculations and data are at constant atmospheric pressure.

The solubilities in ethanol, propan-1-ol, butan-1-ol, and 2-butanol are presented in Fig. 9; those in acetone, and butan-2-one in Fig. 10; in ethyl acetate in Fig. 11. The theoretical calculations carried out using the SAFT-γ Mie approach are compared with the experimental results of our current work (cf. Fig. 3) as well as those found in the literature [16, 89, 91, 92, 93, 94].

In comparing the three substances, it is interesting to note that the solubilities of benzoic acid and diphenylamine in alcohols are very similar (e.g., compare at $T = 300$ K, in Fig. 9), but the solubility of diphenylamine is considerably higher than that of benzoic acid in the ketones (Fig. 10) and esters (Fig. 11) studied. The change of curvature of the solubility of diphenylamine seen in Fig. 9 at temperatures close to 323 K is characteristic of solid-liquid equilibria close to being solid-liquid-liquid equilibria in the phase diagram. By contrast, the solubility of mefenamic acid is clearly much lower in all of the solvents. It is also worth noting the very good overall agreement obtained between the SAFT-γ Mie calculations and the experimental data.

We present phase diagrams of the mixture of benzoic acid and water in Fig. 12 (at (a) $P = 1$ bar, and (b) $T = 413.65$ K). The solid-liquid equilibrium is shown in Fig. 12 (a), where the excellent agreement between SAFT-γ Mie calculations and experimental data of reference mentioned in Table 8 can be seen. Three-phase solid-liquid-liquid phase coexistence is observed at 369 K both in experimental measurements [95] and in our SAFT-γ Mie prediction. An excellent agreement is also obtained for the prediction of the bubble pressure of the mixture of benzoic acid and water at $T = 413.65$ K. The full prediction of the vapour-liquid equilibrium is shown both in Fig. 12 (a) and (b). Most of the experimental points of the liquid-liquid equilibrium correspond to metastable states [95, 96]. The prediction of the liquid-liquid equilibrium with SAFT-γ Mie is qualitatively correct, although we noet the overestimation of the critical

temperature of the liquid-liquid equilibrium envelope.

In Fig. 13 a mixed-solvent system is studied. SAFT-γ Mie predicted solubilities in a binary mixture of water+ethanol are compared with experimental data available in the literature [94, 89, 5]. We emphasise at this point the fact that mixed-solvent data were not used to characterise the the group interactions, and so the calculations presented in this figure are entirely predictive. We have previously shown that very good agreement with experimental data for the solubility of benzoic acid in pure water (cf. Fig. 12 (a)) and pure ethanol (cf. Fig. 9(a)) is obtained with our model. In order to examine the ternary mixture of benzoic acid + water + ethanol it is useful however to define a solvent mole fraction in terms of the composition of ethanol and water only, i.e., $\chi_{\text{ethanol}} = \dfrac{x_{\text{ethanol}}}{x_{\text{water}} + x_{\text{ethanol}}}$ and $\chi_{\text{water}} = \dfrac{x_{\text{water}}}{x_{\text{water}} + x_{\text{ethanol}}}$, which satisfy: $\chi_{\text{water}} + \chi_{\text{ethanol}} = 1$ (note that solubility mole fraction $x^{\text{sat}}_{\text{BA}}$ of benzoic acid also satisfies $x_{\text{water}} + x_{\text{ethanol}} + x^{\text{sat}}_{\text{BA}} = 1$). The solubility $x^{\text{sat}}_{\text{BA}}$ of benzoic acid in water+ethanol predicted by SAFT-γ Mie is shown in Fig. 13 as a function of χ_{ethanol}. As can be seen the solubility $x^{\text{sat}}_{\text{BA}}$ increases close to linearly for an increase of χ_{ethanol}. A very good agreement is found between the prediction of SAFT-γ Mie and the experimental data [94].

In the case of the solubility of diphenylamine in pure water, the data found in the literature [97, 89, 98, 99] are not found to be consistent enough to be used for parameter estimation; instead we apply combining rules to treat the aCNHaC-H_2O unlike interactions. With this, a predictive calculation of the solubility of diphenylamine in water+ethanol, shown in Fig. 13 can be carried out. The calculations are found to overestimate the experimental solubility [89]. in the the higher ethanol mole fractions. SAFT-γ Mie however predicts very well the qualitative evolution of the solubility of diphenylamine in water+ethanol as a function of the solvent mole fraction: the solubility is very low in the water-rich solutions ($\chi_{\text{ethanol}} < 0.5$), becoming significant, in ethanol-rich solutions for $\chi_{\text{ethanol}} > 0.5$.

Similarly, the solubility of mefenamic acid is known to be several orders of magnitude smaller in water than in organic solvents [5, 16]. In the inset of

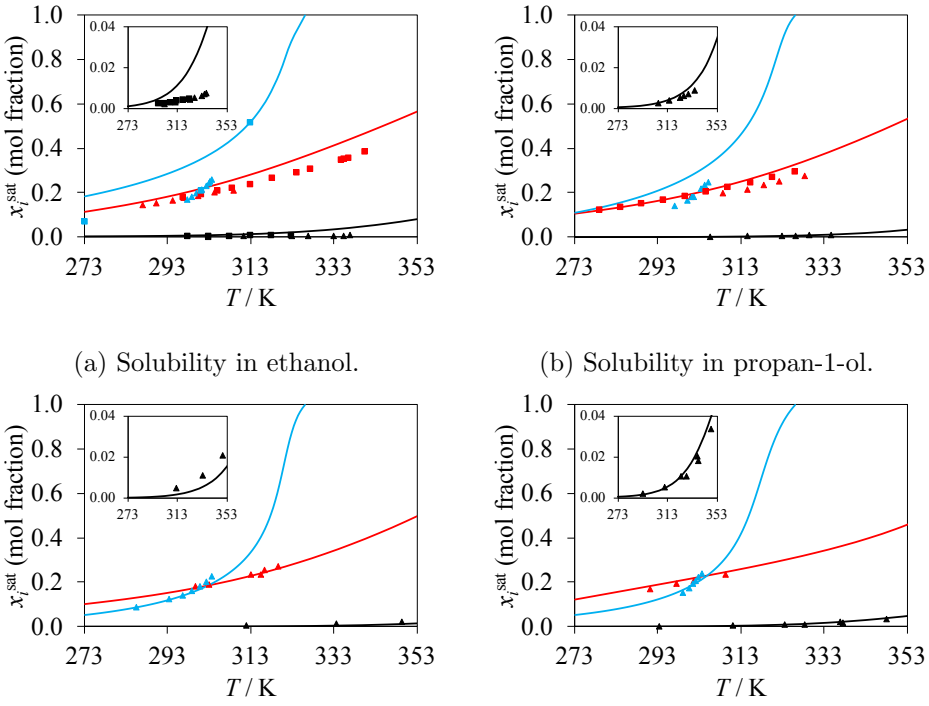

(a) Solubility in ethanol.

(b) Solubility in propan-1-ol.

(c) Solubility in butan-1-ol.

(d) Solubility in butan-2-ol.

Figure 9: Solubility x_i^{sat} of compounds i: benzoic acid (red), diphenylamine (blue), and mefenamic acid (black) in alcohols. The curves represent the solubility calculated with SAFT-γ Mie. The triangles represent the experimental results presented in our work. The squares represent the solubility measured in previous work and found in the literature, for (a) benzoic acid in ethanol [91], diphenylamine in ethanol [89], mefenamic acid in ethanol [16], and (b) benzoic acid in propan-1-ol [92].

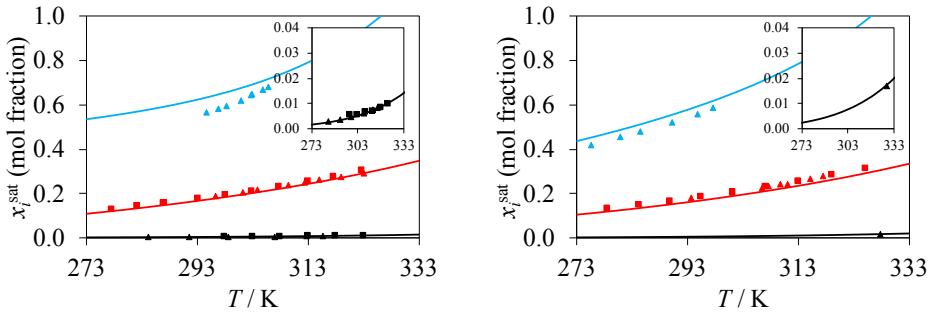

(a) Solubility in acetone.

(b) Solubility in butan-2-one.

Figure 10: Solubility x_i^{sat} of compounds i: benzoic acid (red), diphenylamine (blue), and mefenamic acid (black) in ketones. The curves represent the solubility calculated with SAFT-γ Mie. The triangles represent the experimental results presented in our work. The squares represent the solubility measured in previous work and found in the literature, for (a) benzoic acid in acetone [93], mefenamic acid in acetone [16], and (b) benzoic acid in butan-2-one [92].

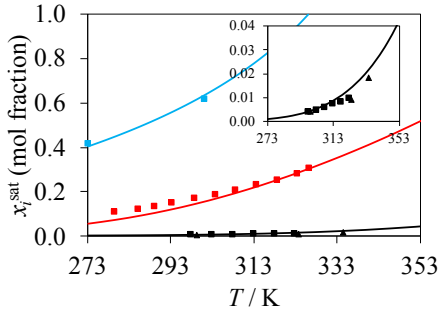

Figure 11: Solubility x_i^{sat} of compounds i: benzoic acid (red), diphenylamine (blue), and mefenamic acid (black) in ethyl acetate. The curves represent the solubility calculated with SAFT-γ Mie. The triangles represent the experimental results presented in our work. The squares represent the solubility measured in previous work and found in the literature, for benzoic acid [92], diphenylamine [89], and mefenamic acid [16] in ethyl acetate.

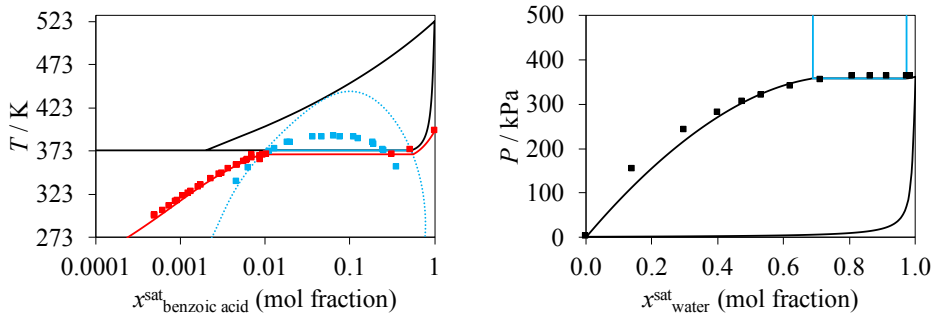

(a) $P = 1$ bar (b) $T = 413.65$ K

Figure 12: Phase diagrams of the mixture of benzoic acid and water at (a) $P = 1$ bar, and (b) $T = 413.65$ K. The curves represent the solid-liquid (red), liquid-liquid (blue), and vapour-liquid (black) phase boundary curves calculated with SAFT-γ Mie, at equilibrium (continuous curves), and for metastable phases (dashed curve). The squares represent experimental results found in the literature for the solid-liquid [95, 83] , liquid-liquid [95, 96], and vapour-liquid [100] equilibria. Similar figures can be found in Reference [101] with PC-SAFT calculations.

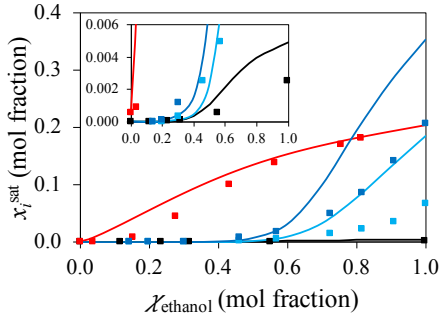

Figure 13: Solubility x_i^{sat} of compounds i: benzoic acid at $T = 298.15$ K (red), diphenylamine at $T = 273.15$ K (light blue), and at $T = 301.15$ K (dark blue), and mefenamic acid at $T = 298.15$ K (black) in water + ethanol. The curves represent the solubility calculated with SAFT-γ Mie. The squares correspond to experimental literature data for benzoic acid [94], diphenylamine [89], and mefenamic acid [5], respectively. The solubility x_i^{sat} is the mole fraction of i in the ternary mixture (i + water + ethanol), as $x_{\text{water}} + x_{\text{ethanol}} + x_i^{\text{sat}} = 1$. The solvent mole fraction χ_{ethanol} is given by $\chi_{\text{ethanol}} = \dfrac{x_{\text{ethanol}}}{x_{\text{water}} + x_{\text{ethanol}}}$.

Fig. 13, we show that the solubility of mefenamic acid in water+ethanol is very small in water-rich mixtures, for $\chi_{\text{ethanol}} < 0.5$, and increases for $\chi_{\text{ethanol}} > 0.5$ in ethanol-rich mixtures. The prediction of SAFT-γ Mie overestimates the solubility of mefenamic acid in ethanol-rich solutions, compared to experiment [5], but the order of magnitude of the prediction is correct (Fig. 9(a)).

4. Conclusions

The experimental results and the group contribution approach shown in our current work extend our understanding of the thermodynamic properties of benzoic acid, diphenylamine, and mefenamic acid. We present the solubility as a key property in our study, due to its role in pharmaceutical processes and drug manufacturing, and we emphasise the interest in predicting solubility of active pharmaceutical ingredients in different solvent families. In this context, we demonstrate how the SAFT-γ Mie approach constitutes a well-suited approach to predict solubility and aid in solvent selection.

We present new experimental solubility data for benzoic acid, diphenylamine, and mefenamic acid, in alcohols, ketones, and esters. Before our current work, only a few solubility data for mefenamic acid was available in the literature, e.g. in Mudalip et al. [16]. We extend the applicability of the SAFT-γ Mie equation of state by introducing two new groups: the aCCOOH group for benzoic acid and related molecules, and the aCNHaC group for diphenylamine and related molecules. Both aCCOOH and aCNHaC groups are used in the molecular modelling of mefenamic acid. We also define the CH_3CO group for 2-ketones to extend the SAFT-γ Mie applicability in describing the ketone family as solvents. We use the new solubility data presented in our current work, together with reference data found in the literature, to estimate the parameters of the new group-group interactions and to assess the accuracy of the predictions of the models developed.

The new solubility measurements are found to be consistent with the few available data of the literature. The solubility of mefenamic acid is always

smaller than the solubility of benzoic acid and diphenylamine, for a given temperature and solvent, as it can be expected from the complexity of the molecular structures of the molecules and their melting temperatures. The order of magnitude of the solubility of benzoic acid and diphenylamine in alcohols is, by contrast, similar. The solubility curves as a function of temperature for these compounds are seen to cross: for $T < 300$ K, the solubility of benzoic acid is generally slightly higher than the solubility of diphenylamine, and it is the opposite for $T > 300$ K. In ketones, the solubility of diphenylamine is found to be significantly higher than the solubility of benzoic acid.

We obtain an excellent agreement between the SAFT-γ Mie calculations and the experimental data selected for parameter estimation, which demonstrates that the theoretical approach is well-suited for the description of the thermodynamic properties of interest here: vapour pressure, saturated density, enthalpy of vapourisation, bubble temperature, dew temperature, bubble pressure, and solid-liquid solubility. The uncertainty in experimental data used for comparison is often not reported, which hinders the validation of the model predictions. We present %AADs, AADs, parity plots, solid-liquid solubility phase diagrams, in order to provide an indication of the accuracy of the theoretical calculations and predictions

The new groups identified are transferable to other molecules, in particular to other non-steroidal anti-inflammatory drugs, which incorprate the same aCCOOH and aCNHaC groups, and to solvents including the CH_3CO group. Several refinements will be considered in further studies. Intramolecular hydrogen bonding interactions can be included in the molecular modelling and used both in parameter estimation and prediction [54, 102]. Taking into account intramolecular hydrogen bonds would allow to differentiate Form I and Form II of mefenamic acid in the model, and hence distinguish their calculated solubility. Further improvement can be expected for the description of the unlike interaction between water and the aCNHaC group. We have treated this interaction here using combining rules, in future, with the aid of more experimental data this interaction should be further refined.

Acknowledgements

We acknowledge support from the EPSRC and the Future Manufacturing Research Hub in Continuous Manufacturing and Advanced Crystallization (Grants ref: EP/P006965/1 and EP/I033459/1) for funding this work. The experimental work was carried out in the CMAC National Facility, housed within the University of Strathclyde's Technology and Innovation Centre, supported by the UKRPIF (UK Research Partnership Investment Fund) award from the Higher Education Funding Council for England (HEFCE) (Grant ref: HH13054). We also acknowledge financial support from the Engineering and Physical Sciences Research Council (EPSRC) of the UK (grants GR/T17595, GR/N35991, EP/E016340, EP/P006965, and EP/J014958) to the Molecular Systems Engineering group. Amparo Galindo is thankful to the Royal Academy of Engineering and Eli Lilly and Company for support of a Research Chair (Grant RCSRF18193).

Experimental solubilities for mefenamic acid in propan-1-ol, butan-1-ol, butan-2-ol, pentan-2-ol, butan-2-one, pentan-2-one, ethyl acetate, butyl acetate, and isopropyl acetate were determined as part of a CMAC pre-competitive Core Project; the authors would like to thank the CMAC Tier 1 companies GlaxoSmithKline, AstraZeneca, Novartis, Bayer AG, Eli Lilly and Company, Takeda, Roche and Pfizer for funding and supporting this work.

Supplementary information

Additional tables and figures are provided in the supplementary information, with corresponding literature sources given in references [103, 92, 104, 105, 106, 107, 108, 109, 110, 94, 111, 78, 79, 112, 93, 81, 80, 113, 82, 114, 115, 116, 83, 89, 117, 16, 5, 118].

Data statement

Data underlying this article can be accessed on Zenodo at https://zenodo.org/record/xxxxxx, and used under the Creative Commons Attribution license.

References

[1] C. J. Brown, S. McGlone, T. Yerdelen, V. Srirambhatla, F. Mabbott, R. Gurung, M. L. Briuglia, B. Ahmed, H. Polyzois, J. McGinty, F. Perciballi, D. Fysikopoulos, P. MacFhionnghaile, H. Siddique, V. Raval, T. S. Harrington, A. D. Vassileiou, M. Robertson, E. Prasad, A. Johnston, B. Johnston, A. Nordon, J. Srai, G. Halbert, J. H. ter Horst, C. J. Price, C. D. Rielly, J. Sefcik, A. J. Florence, Enabling precision manufacturing of active pharmaceutical ingredients: workflow for seeded cooling continuous crystallisations, Mol. Syst. Des. Eng. 3 (2018) 518–549. doi:10.1039/C7ME00096K.

[2] A. B. Anderson, P. J. Haynes, J. Guillebaud, A. C. Turnbull, Reduction of menstrual blood-loss by prostaglandin-synthetase inhibitors, The Lancet 307 (7963) (76) 774–776. doi:10.1016/s0140-6736(76)91612-3.

[3] T. Pringsheim, W. J. Davenport, D. Dodick, Acute treatment and prevention of menstrually related migraine headache, Neurology 70 (17) (2008) 1555–1563. doi:10.1212/01.wnl.0000310638.54698.36.

[4] http://www.medicines.org.uk, accessed in november 2020.

[5] S. Romero, B. Escalera, P. Bustamente, Solubility behavior of polymorphs I and II of mefenamic acid in solvent mixtures, Int. J. Pharm. 178 (2) (1999) 193–202. doi:10.1016/S0378-5173(98)00375-5.

[6] R. Panchagnula, P. Sundaramurthy, O. Pillai, S. Agrawal, Y. A. Raj, Solid-state characterization of mefenamic acid, J. Pharm. Sci. 93 (4) (2004) 1019–29. doi:10.1002/jps.20008.

[7] F. Kato, M. Otsuka, Y. Matsuda, Kinetic study of the transformation of mefenamic acid polymorphs in various solvents and under high humidity conditions, Int. J. Pharm. 321 (1–2) (2006) 18–26. doi:10.1016/j.ijpharm.2006.04.020.

[8] S. Cesur, S. Gokbel, Crystallization of mefenamic acid and polymorphs, Cryst. Res. Technol. 43 (7) (2008) 720–728. doi:10.1002/crat.200711119.

[9] S. SeethaLekshmi, T. N. Guru Row, Conformational polymorphism in a non-steroidal anti-inflammatory drug, mefenamic acid, Cryst. Growth Des. 12 (8) (2012) 4283–4289. doi:10.1021/cg300812v.

[10] V. R. R. Cunha, C. M. S. Izumi, P. A. D. Petersen, A. Magalhães, M. L. A. Temperini, H. M. Petrilli, V. R. L. Constantino, Mefenamic acid anti-inflammatory drug: probing its polymorphs by vibrational (IR and Raman) and solid-state NMR spectroscopies, J.Phys.Chem. B 118 (16) (2014) 4333–4344. doi:10.1021/jp500988k.

[11] K. Sypek, I. S. Burns, A. J. Florence, J. Sefcik, In situ monitoring of stirring effects on polymorphic transformations during cooling crystallization of carbamazepine, Cryst. Growth Des. 12 (10) (2012) 4821–4828. doi:10.1021/cg3005689.

[12] N. E. B. Briggs, U. Schacht, V. Raval, T. McGlone, J. Sefcik, A. J. Florence, Seeded crystallization of β-l-glutamic acid in a continuous oscillatory baffled crystallizer, Org. Process Res. Dev. 19 (12) (2015) 1903–1911. doi:10.1021/acs.oprd.5b00206.

[13] U. Domańska, A. Pobudkowska, A. Pelczarska, M. Winiarska-Tusznio, P. Gierycz, Solubility and pKa of select pharmaceuticals in water, ethanol, and 1-octanol, J. Chem. Thermodyn. 42 (12) (2010) 1465–1472. doi:10.1016/j.jct.2010.07.001.

[14] U. Domańska, A. Pobudkowska, A. Pelczarska, Solubility of sparingly soluble drug derivatives of anthranilic acid, J. Phys. Chem. B 115 (11) (2011) 2547–54. doi:10.1021/jp109905r.

[15] A. Zeinolabedini Hezave, M. H. Khademi, F. Esmaeilzadeh, Measurement and modeling of mefenamic acid solubility in supercritical carbon dioxide,

Fluid Phase Equilib. 313 (2012) 140–147. doi:10.1016/j.fluid.2011.09.031.

[16] S. K. A. Mudalip, M. R. A. Bakar, P. Jamal, F. Adam, Solubility and dissolution thermodynamic data of mefenamic acid crystals in different classes of organic solvents, J. Chem. Eng. Data 58 (12) (2013) 3447–3452. doi:10.1021/je400714f.

[17] W. G. Chapman, K. E. Gubbins, G. Jackson, M. Radosz, SAFT: Equation-of-state solution model for associating fluids, Fluid Phase Equilib. 52 (1989) 31–38. doi:http://dx.doi.org/10.1016/0378-3812(89)80308-5.

[18] W. G. Chapman, K. E. Gubbins, G. Jackson, M. Radosz, New reference equation of state for associating liquids, Ind. & Eng. Chem. Res. 29 (8) (1990) 1709–1721. doi:10.1021/ie00104a021.

[19] G. Jackson, W. G. Chapman, K. E. Gubbins, Phase equilibria of associating fluids: Spherical molecules with multiple bonding sites, Mol. Phys. 65 (1) (1988) 1–31. doi:10.1080/00268978800100821.

[20] W. G. Chapman, G. Jackson, K. E. Gubbins, Phase equilibria of associating fluids, Mol. Phys. 65 (5) (1988) 1057–1079. doi:10.1080/00268978800101601.

[21] A. Gil-Villegas, A. Galindo, P. J. Whitehead, S. J. Mills, G. Jackson, A. N. Burgess, Statistical associating fluid theory for chain molecules with attractive potentials of variable range, J. Chem. Phys. 106 (10) (1997) 4168–4186. doi:doi:http://dx.doi.org/10.1063/1.473101.

[22] F. J. Blas, L. F. Vega, Thermodynamic behaviour of homonuclear and heteronuclear lennard-jones chains with association sites from simulation and theory, Mol. Phys. 92 (1) (1997) 135–150. doi:10.1080/002689797170707.

[23] J. C. Pàmies, L. F. Vega, Vapor-liquid equilibria and critical behavior of heavy n-alkanes using transferable parameters from the soft-saft equation of state, Ind. Eng. Chem. Res. 40 (11) (2001) 2532–2543. doi:10.1021/ie000944x.

[24] F. Llovell, J. C. Pàmies, L. F. Vega, Thermodynamic properties of Lennard-Jones chain molecules: Renormalization-group corrections to a modified statistical associating fluid theory, J. Chem. Phys. 121 (21) (2004) 10715–10724. doi:10.1063/1.1809112.

[25] F. Llovell, L. F. Vega, Global fluid phase equilibria and critical phenomena of selected mixtures using the crossover soft-SAFT equation, J. Phys. Chem. B 110 (3) (2006) 1350–1362. doi:10.1021/jp0551465.

[26] F. Llovell, L. F. Vega, Prediction of thermodynamic derivative properties of pure fluids through the soft-SAFT equation of state, J. Phys. Chem. B 110 (23) (2006) 11427–11437. doi:10.1021/jp0608022.

[27] T. Lafitte, A. Apostolakou, C. Avendaño, A. Galindo, C. S. Adjiman, E. A. Müller, G. Jackson, Accurate statistical associating fluid theory for chain molecules formed from Mie segments, J. Chem. Phys. 139 (15) (2013) 154504. doi:10.1063/1.4819786.

[28] J. Gross, G. Sadowski, Perturbed-Chain SAFT: An equation of state based on a perturbation theory for chain molecules, Ind. Eng. Chem. Res. 40 (4) (2001) 1244–1260. doi:10.1021/ie0003887.

[29] L. F. Cameretti, G. Sadowski, J. M. Mollerup, Modeling of aqueous electrolyte solutions with perturbed-chain statistical associated fluid theory, Ind. Eng. Chem. Res. 44 (9) (2005) 3355–3362. doi:10.1021/ie0488142.

[30] N. Haarmann, R. Siewert, A. A. Samarov, S. P. Verevkin, C. Held, G. Sadowski, Thermodynamic Properties of Systems Comprising Esters: Experimental Data and Modeling with PC-SAFT and SAFT-γ Mie, Ind. Eng. Chem. Res. 58 (16) (2019) 6841–6849. doi:10.1021/acs.iecr.9b00714.

[31] F. Ruether, G. Sadowski, Modeling the solubility of pharmaceuticals in pure solvents and solvent mixtures for drug process design, J. Pharm. Sci. 98 (11) (2009) 4205–4215. doi:https://doi.org/10.1002/jps.21725.

[32] T. Spyriouni, X. Krokidis, I. G. Economou, Thermodynamics of pharmaceuticals: Prediction of solubility in pure and mixed solvents with PC-SAFT, Fluid Phase Equilib. 302 (1) (2011) 331–337. doi:10.1016/j.fluid.2010.08.029.

[33] B. Bouillot, T. Spyriouni, S. Teychené, B. Biscans, Solubility of pharmaceuticals: A comparison between SciPharma, a PC-SAFT-based approach, and NRTL-SAC, Eur. Phys. J. Spec. Top. 226 (2017) 913–929. doi:10.1140/epjst/e2016-60225-5.

[34] D. Fuchs, J. Fischer, F. Tumakaka, G. Sadowski, Solubility of Amino Acids: Influence of the pH value and the Addition of Alcoholic Cosolvents on Aqueous Solubility, Ind. Eng. Chem. Res. 45 (19) (2006) 6578–6584. doi:10.1021/ie0602097.

[35] J. Cassens, A. Prudic, F. Ruether, G. Sadowski, Solubility of Pharmaceuticals and Their Salts As a Function of pH, Ind. Eng. Chem. Res. 52 (7) (2013) 2721–2731. doi:10.1021/ie302064h.

[36] A. Prudic, Y. Ji, G. Sadowski, Thermodynamic Phase Behavior of API/Polymer Solid Dispersions, Mol. Pharm. 11 (7) (2014) 2294–2304. doi:10.1021/mp400729x.

[37] A. Prudic, Y. Ji, C. Luebbert, G. Sadowsk, Influence of humidity on the phase behavior of API/polymer formulations, Eur. J. Pharm. Biopharm. 94 (2015) 352–362. doi:10.1016/j.ejpb.2015.06.009.

[38] R. Paus, Y. Ji, L. Vahle, G. Sadowski, Predicting the solubility advantage of amorphous pharmaceuticals: A novel thermodynamic approach, Mol. Pharm. 12 (8) (2015) 2823–2833. doi:10.1021/mp500824d.

[39] K. Lehmkemper, S. O. Kyerematen, O. Heinzerling, M. Degenhardt, G. Sadowski, Long-Term Physical Stability of PVP- and PVPVA-Amorphous Solid Dispersions, Mol. Pharm. 14 (1) (2017) 157–171. doi:10.1021/acs.molpharmaceut.6b00763.

[40] K. Lehmkemper, S. O. Kyerematen, O. Heinzerling, M. Degenhardt, G. Sadowski, Impact of polymer type and relative humidity on the long-term physical stability of amorphous solid dispersions, Mol. Pharm. 14 (12) (2017) 4374–4386. doi:10.1021/acs.molpharmaceut.7b00492.

[41] V. Papaioannou, T. Lafitte, C. Avendaño, C. S. Adjiman, G. Jackson, E. A. Müller, A. Galindo, Group contribution methodology based on the statistical associating fluid theory for heteronuclear molecules formed from Mie segments, J. Chem. Phys. 140 (5) (2014) 54107. doi:10.1063/1.4851455.

[42] S. Dufal, T. Lafitte, A. J. Haslam, A. Galindo, G. N. I. Clark, C. Vega, G. Jackson, The A in SAFT: Developing the contribution of association to the Helmholtz free energy within a Wertheim TPT1 treatment of generic Mie fluids, Mol. Phys. 113 (9–10) (2015) 948–984. doi:10.1080/00268976.2015.1029027.

[43] A. J. Haslam, A. Gonzalez-Perez, S. Di Lecce, S. H. Khalit, F. A. Perdomo, S. Kournopoulos, M. Kohns, T. Lindeboom, M. Wehbe, S. A. Febra, G. Jackson, C. S. Adjiman, A. Galindo, Expanding the applications of the SAFT-γ Mie group-contribution equation of state: prediction of thermodynamic properties and phase behaviour of mixtures, submitted to J. Chem. Eng. Data (2020).

[44] E. A. Müller, G. Jackson, Force-field parameters from the SAFT-γ equation of state for use in coarse-grained molecular simulations, Annu. Rev. Chem. Biomol. Eng. 5 (1) (2014) 405. doi:10.1146/annurev-chembioeng-061312-103314.

[45] P. Hutacharoen, S. Dufal, V. Papaioannou, R. M. Shanker, C. S. Adjiman, G. Jackson, A. Galindo, Predicting the Solvation of Organic Compounds in Aqueous Environments: From Alkanes and Alcohols to Pharmaceuticals, Ind. & Eng. Chem. Res. 56 (38) (2017) 10856–10876. doi:10.1021/acs.iecr.7b00899.

[46] S. Di Lecce, G. Lazarou, S. H. Khalit, C. S. Adjiman, G. Jackson, A. Galindo, L. McQueen, Modelling and prediction of the thermophysical properties of aqueous mixtures of choline geranate and geranic acid (CAGE) using SAFT-γ Mie, RSC Adv. 9 (65) (2019) 38017–38031. doi:10.1039/C9RA07057E.

[47] J. Mullin, 3.6 Ideal and non-ideal solutions, in: Crystallization, 4th Edition, Butterworth-Heinemann, Oxford, 2001, pp. 98–100. doi:10.1016/B978-075064833-2/50005-X.

[48] A. Shayanfar, S. Velaga, A. Jouyban, Solubility of carbamazepine, nicotinamide and carbamazepine-nicotinamide cocrystal in ethanol-water mixtures, Fluid Phase Equilib. 363 (2014) 97–105. doi:https://doi.org/10.1016/j.fluid.2013.11.024.

[49] H. T. Do, Y. Z. Chua, A. Kumar, D. Pabsch, M. Hallermann, D. Zaitsau, C. Schick, C. Held, Melting properties of amino acids and their solubility in water, RSC Adv. 10 (2020) 44205–44215. doi:10.1039/D0RA08947H.

[50] S. Dufal, V. Papaioannou, M. Sadeqzadeh, T. Pogiatzis, A. Chremos, C. S. Adjiman, G. Jackson, A. Galindo, Prediction of Thermodynamic Properties and Phase Behavior of Fluids and Mixtures with the SAFT-γ Mie Group-Contribution Equation of State, J. Chem. Eng. Data 59 (10) (2014) 3272–3288. doi:10.1021/je500248h.

[51] S. Dufal, T. Lafitte, A. J. Haslam, A. Galindo, G. N. I. Clark, C. Vega, G. Jackson, Corrigendum: The A in SAFT: Developing the contribution of association to the Helmholtz free energy within a Wertheim TPT1

treatment of generic Mie fluids, Mol. Phys. 116 (2) (2018) 283–285. doi:10.1080/00268976.2017.1402604.

[52] J. Vellema, N. Hunfeld, H. Van den Akker, J. ter Horst, Avoiding crystallization of lorazepam during infusion, Eur. J. Pharm. Sci. 44 (5) (2011) 621–626. doi:https://doi.org/10.1016/j.ejps.2011.10.010.

[53] H. T. Do, Y. Z. Chua, J. Habicht, M. Klinksiek, M. Hallermann, D. Zaitsau, C. Schick, C. Held, Melting properties of peptides and their solubility in water. Part 1: dipeptides based on glycine or alanine, RSC Adv. 9 (2019) 32722–32734. doi:10.1039/C9RA05730G.

[54] S. A. Febra, Ring formation in a statistical associating fluid theory framework, Ph.D. thesis, Imperial College London (2018).

[55] K. Moodley, T. Chetty, D. Ramjugernath, Solid-Liquid Equilibrium Measurements for Posaconazole and Voriconazole in Several Solvents between T = 278.2 and 323.2 K Using Differential Thermal Analysis/Thermal Gravimetric Analysis, J. Chem. Eng. Data 64 (8) (2019) 3367–3374. doi:10.1021/acs.jced.9b00179.

[56] L. Kousková, J. Leitner, Dsc study of the system o-acetylsalicylic acid-caffeine and thermodynamic modelling of the system o-acetylsalicylic acid-caffeine-paracetamol, Thermochim. Acta 674 (2019) 63–67. doi:10.1016/j.tca.2019.02.007.

[57] H. Flores, F. Ramos, E. A. Camarillo, O. Santiago, G. Perdomo, R. Notario, S. Cabrera, Isothermal thermogravimetric study for determining sublimation enthalpies of some hydroxyflavones, J. Chem. Eng. Data 63 (6) (2018) 1925–1936. doi:10.1021/acs.jced.7b01034.

[58] J. M. Fonseca, N. Gushterov, R. Dohrn, Vapour pressures of selected organic compounds down to 1 mPa, using mass-loss Knudsen effusion method, J. Chem. Thermodyn. 73 (2014) 148–155. doi:10.1016/j.jct.2013.11.038.

[59] B. Bouillot, S. Teychené, B. Biscans, An evaluation of cosmo-sac model and its evolutions for the prediction of drug-like molecule solubility: Part 1, Ind. Eng. Chem. Res. 52 (26) (2013) 9276–9284. doi:10.1021/ie3015318.

[60] H. Yang, J. Thati, Å. C. Rasmuson, Thermodynamics of molecular solids in organic solvents, J. Chem. Thermodyn. 48 (2012) 150–159. doi:10.1016/j.jct.2011.12.015.

[61] T.-C. Wang, K.-C. Deng, Solid-liquid equilibria for three binary mixtures of benzoic acid with heptanedioic acid, 3-methylpentanedioic acid, and 2,3-dimethylbutanedioic acid, J. Chem. Eng. Data 57 (1) (2012) 78–81. doi:10.1021/je200681k.

[62] S. Chelouche, D. Trache, S. ao P. Pinho, K. Khimeche, Experimental and modeling studies of binary organic eutectic systems to be used as stabilizers for nitrate esters-based energetic materials, Fluid Phase Equilib. 498 (2019) 104–115. doi:10.1016/j.fluid.2019.06.021.

[63] D. Trache, K. Khimeche, A. Dahmani, Study of (solid-liquid) phase equilibria for mixtures of energetic material stabilizers and prediction for their subsequent performance, Int. J. Thermophys. 34 (2013) 226–239. doi:10.1007/s10765-013-1404-4.

[64] B. Sharma, P. Lal, M. Sharma, A. Sharma, Thermoanalysis of binary condensed eutectic phases evincing molecular interactions, J. Therm. Anal. Calorim. 109 (2013) 447–456. doi:10.1007/s10973-011-1673-8.

[65] A. Mekki, K. Khimeche, A. Dahmani, Measurement and prediction of (solid+liquid) equilibria of gun powder's and propellant's stabilizers mixtures, J. Chem. Thermodyn. 42 (8) (2010) 1050–1055. doi:10.1016/j.jct.2010.03.025.

[66] A. O. Surov, I. V. Terekhova, A. Bauer-Brandl, G. L. Perlovich, Ther-

modynamic and structural aspects of some fenamate molecular crystals, Cryst. Growth Des. 9 (7) (2009) 3265–3272. doi:10.1021/cg900002q.

[67] D. Hopfe, Thermophysical data of pure substances, Data Compilation of FIZ CHEMIE Germany (1990) 1.

[68] J. Donnelly, L. Drewes, R. Johnson, W. Munslow, K. Knapp, G. Sovocool, Purity and heat of fusion data for environmental standards as determined by differential scanning calorimetry, Thermochim. Acta 167 (2) (1990) 155–187. doi:10.1016/0040-6031(90)80476-F.

[69] B. Bouillot, Approches thermodynamiques pour la prédiction de la solubilité de molécules d'intérêt pharmaceutique, Phd thesis, Université de Toulouse (2011).

[70] V. Papaioannou, F. Calado, T. Lafitte, S. Dufal, M. Sadeqzadeh, G. Jackson, C. S. Adjiman, A. Galindo, Application of the SAFT-γ Mie group contribution equation of state to fluids of relevance to the oil and gas industry, Fluid Phase Equilib. 416 (2016) 104–119. doi:10.1016/j.fluid.2015.12.041.

[71] P. Hutacharoen, Prediction of Partition Coefficients and Solubilities of Active Pharmaceutical Ingredients with the SAFT-γ Mie Group-contribution Approach, Ph.D. thesis, Imperial College London (2017).

[72] F. Perdomo, S. Khalit, C. S. Adjiman, A. Galindo, G. Jackson, Description of thermodynamic properties and fluid-phase behaviour of aqueous solutions of linear, branched, and cyclic amines, submitted to AIChE J.; under review (2020).

[73] K. Kroenlein, C. Muzny, A. Kazakov, V. Diky, R. Chirico, J. Magee, I. Abdulagatov, M. Frenkel, NIST Standard Reference 203: TRC Web Thermo Tables (WTT) Version 2-2012-1 Professional.
URL https://wtt-pro.nist.gov/wtt-pro/

[74] L. Wang, R. Ouyang, E. Al., Vapor-Liquid Equilibrium for System Toluene - Benzaldehyde - Benzoic Acid, Huaxue Gongcheng Xi'an 20 (6) (1992) 45–53.

[75] V. E. Abramov, N. A. Smirnova, Liquid-vapor equilibrium in systems containing semi-products of the synthesis of benzoic acid. Part 4, Deposited Doc. Oniitekhim (1989) 1–21.

[76] K. Doering, Vapor pressures of mixtures toluene - benzoic acid, Tech. rep., FIZ Report (1965).

[77] A. de Haan, B. Nienhaus, J. Gmehling, Detherm (1996).

[78] M. Roloff, Contributions to the Knowledge of Cryo-Hydrates, Z. Phys. Chem. NF 17U (1) (1895) 325–356.

[79] J. Chipman, Solubilities of Inorganic and Organic Compounds, J. Am. Chem. Soc. 46 (11) (1924) 2445–2448.

[80] J. Thati, F. L. Nordström, Å. C. Rasmuson, Solubility of Benzoic Acid in Pure Solvents and Binary Mixtures, J. Chem. Eng. Data 55 (11) (2010) 5124–5127. doi:10.1021/je100675r.

[81] A. Książczak, Solid-liquid equilibrium and the structure of solutions of highly polar aromatic compounds, Fluid Phase Equilib. 28 (1) (1986) 57–72. doi:10.1016/0378-3812(86)85068-3.

[82] W. E. Acree, G. L. Bertrand, Thermochemical Investigations of Nearly Ideal Binary Solvents VII: Monomer and Dimer Models for Solubility of Benzoic Acid in Simple Binary and Ternary Solvents, J. Pharm. Sci. 70 (9) (1981) 1033–1036. doi:10.1002/JPS.2600700917.

[83] G. Ren, J. Wang, G. Li, Solubility of paroxetine hydrochloride hemihydrate in (water + acetone), J. Chem. Thermodyn. 37 (8) (2005) 860–865. doi:10.1016/j.jct.2004.12.006.

[84] D. Q. Li, D. Z. Liu, F. A. Wang, Solubility of 4-methylbenzoic acid between 288 K and 370 K, J. Chem. Eng. Data 46 (2) (2001) 234–236. doi:10.1021/je000202a.

[85] V. Marinin, Supersonic Velocity in Liquids and Solutions, Zh. Fiz. Khim. 25 (6) (1951) 641–646.

[86] G. A. Barclay, R. J. W. Le Frève, B. M. Smythe, The variation of dipole moment with state for n-propyl-and n-butyl-amines with notes on the apparent moments in solution of certain other amines, Trans. Faraday Soc. 47 (1951) 357–365.

[87] N. J. Leonard, L. E. Sutton, The Use of Fluoro Compounds in the Determination of Valency Angles by Electric Dipole Moment Measurements (1948). doi:10.1021/ja01184a082.

[88] C. W. N. Cumper, A. P. Thurston, Electric dipole moments and molecular conformations of aromatic amines, phosphites, and phosphates, J. Chem. Soc. B: Physical Organic (1971) 422–426doi:10.1039/j29710000422.

[89] L. Desvergnes, Solubilité de la diphenylamine dans l'eau, dans l'alcool et dans les autres solvants organiques, Ann. Chim. Anal. Chim. Appl. 10 (9) (1928) 253–255.

[90] G. Liessmann, W. Schmidt, S. Reiffarth, Recommended thermophysical data, Data Compilation of the Saechische Olefinwerke Boehlen, Germany (1995).

[91] Y. Li, P.-S. Ma, M.-m. Chen, Y. Liang, J.-F. Wang, Determination and correlation of the solubilities with the ethanol as solvent and the main components of pure terephthalic acid manufacture residue as solute, Journal of Chemical Engineering of Chinese Universities 20 (2006) 282–286.

[92] G. Tully, G. Hou, B. Glennon, Solubility of benzoic acid and aspirin in pure solvents using focused beam reflective measurement, J. Chem. Eng. Data 61 (1) (2016) 594–601. doi:10.1021/acs.jced.5b00746.

[93] B. Long, J. Li, R. Zhang, L. Wan, Solubility of benzoic acid in acetone, 2-propanol, acetic acid and cyclohexane: Experimental measurement and thermodynamic modeling, Fluid Phase Equilib. 297 (1) (2010) 113–120. doi:https://doi.org/10.1016/j.fluid.2010.06.021.

[94] A. Seidell, The solubilities of the pharmaceutical organic acids and their salts, Hygienic Lab. Bull. 67 (1910) 1–93.

[95] H. L. Ward, S. S. Cooper, The system benzoic acid, orthophthalic acid, water, J. Phys. Chem. 34 (7) (1930) 1484–1493. doi:10.1021/j150313a009.

[96] W. Alexejew, Ueber Lösungen, Wied. Ann. XXVIII (1886) 305.

[97] W. M. Dehn, Comparative solubilities in water, in pyridine and in aqueous pyridine., J. Am. Chem. Soc. 39 (7) (1917) 1399–1404. doi:10.1021/ja02252a012.

[98] A. Akbaev, Copper II Chloride-Diphenylamine-Water System at 30°C, Russ. J. Inorg. Chem. 16 (11) (1971) 1681–1682.

[99] D. Mohan Murali Rao, C. Kalidas, Protonation behaviour of diphenylamine in water-dimethyl-formamide (DMF) mixtures, Bull. Soc. Chim. Belg. 98 (6) (1989) 363–366. doi:10.1002/bscb.19890980602.

[100] J. Gmehling, O. U., Vapor-liquid Equilibrium Data Collection, Chemistry Data Series. Frankfurt Main: DECHEMA I (1d) (2003) 186.

[101] T. Reschke, K. V. Zherikova, S. P. Verevkin, C. Held, Benzoic Acid and Chlorobenzoic Acids: Thermodynamic Study of the Pure Compounds and Binary Mixtures With Water, J. Pharm. Sci. 105 (3) (2016) 1050–1058. doi:10.1016/j.xphs.2015.12.020.

[102] S. A. Febra, A. Aasen, C. S. Adjiman, G. Jackson, A. Galindo, Intramolecular bonding in a statistical associating fluid theory of ring aggregates Intramolecular bonding in a statistical associating fluid theory of ring aggregates, Mol. Phys. (22) (2019). doi:10.1080/00268976.2019.1671619.

[103] V. F. Sergeeva, L. A. Eskaraeva, I. Z. Usmanova, V. A. Glybovskaya, Equilibrium of liquid phases in systems of cyclohexane and methanol with naphthalene, with diphenylamine, and with benzoic acid, J. Gen. Chem. USSR 41 (9) (1971) 1908–1911.

[104] Y. Li, P. S. Ma, M. M. Chen, Y. Liang, J. F. Wang, Determination and Correlation of the Solubilities with the Ethanol as Solvent and the Main Components of Pure Terephthalic Acid Manufacture Residue as Solute, Gaoxiao Huaxue Gongcheng Xuebao 20 (2) (2006) 282–286.

[105] J. Jessy, Quantitative correlation of the effect of changing alkyl substitution in solvent, on solubility for alcoholic solutions, J. Indian Chem. Soc. 75 (6) (1998) 352–353.

[106] A. Beerbower, P. L. Wu, A. Martin, Expanded Solubility Parameter Approach I: Naphthalene and Benzoic Acid in Individual Solvents, J. Pharm. Sci. 73 (2) (1984) 179–188. doi:10.1002/jps.2600730210.

[107] F. A. Restaino, A. N. Martin, Solubility of benzoic acid and related compounds in a series of n-alkanols, J. Pharm. Sci. 53 (6) (1964) 636–639. doi:10.1002/jps.2600530613.

[108] C. R. Daniels, A. K. Charlton, R. M. Wold, E. Pustejovsky, A. N. Furman, A. C. Bilbrey, J. N. Love, J. A. Garza, W. E. Acree Jr., Solubility of benzilic acid in select organic solvents at 298.15 k, Phys. Chem. Liq. 41 (6) (2003) 599–603. doi:10.1080/0031910031000162254.

[109] G. L. Perlovichl, A. Bauer-Brandl, Thermodynamics of solutions I: benzoic acid and acetylsalicylic acid as models for drug substances and the prediction of solubility, Pharm. res. 20 (3) (2003) 471–478. doi:10.1023/a:1022624725495.

[110] J. Qingzhu, M. Peisheng, Y. Shouzhi, W. Qiang, W. Chang, L. Guiju, Solubilities of benzoic acid, p-methylbenzoic acid, m-methylbenzoic acid, o-methylbenzoic acid, p-hydroxybenzoic acid, and o-nitrobenzoic acid in

1-octanol, J. Chem. Eng. Data 53 (6) (2008) 1278–1282. doi:10.1021/je700677d.

[111] K. Sandeepa, K. Ravi Kumar, T. S. V. R. Neeharika, B. Satyavathi, P. K. Thella, Solubility measurement and thermodynamic modeling of benzoic acid in monosolvents and binary mixtures, J. Chem. Eng. Data 63 (6) (2018) 2028–2037. doi:10.1021/acs.jced.8b00025.

[112] N. V. Sidgwick, E. K. Ewbank, Cvii.–the influence of position on the solubilities of the substituted benzoic acids, J. Chem. Soc., Trans. 119 (1921) 979–1001. doi:10.1039/CT9211900979.

[113] H.-M. Lin, R. A. Nash, An experimental method for determining the hildebrand solubility parameter of organic nonelectrolytes, J. Pharm. Sci. 82 (10) (1993) 1018–1026. doi:10.1002/jps.2600821009.

[114] P. G. Desai, A. M. Patel, Effect of polarity on the solubilities of some organic acids, J. Indian Chem. Soc. 12 (2) (1935) 131–136.

[115] I. A. Sedov, T. M. Salikov, D. R. Khaibrakhmanova, A. Wadawadigi, O. Zha, E. Qian, E. Hart, M. Barrera, J. Acree, W. E., M. H. Abraham, Determination of abraham model correlations for solute transfer into propyl acetate based on experimental activity coefficient and solubility data, J. Solution Chem. 47 (4) (2018) 634–653. doi:10.1007/s10953-018-0743-y.

[116] S. Zhao, W. Chen, Q. Dai, L. Wang, Solubilities of benzene carboxylic acids in isobutyl acetate from (299.73 to 353.15) K, J. Chem. Eng. Data 56 (5) (2011) 2399–2402. doi:10.1021/je101319f.

[117] M. Étard, Recherches expérimentales sur les solutions saturées, Ann. Chim. Phys. 2 (7) (1894) 570.

[118] K. Park, J. M. B. Evans, A. S. Myerson, Determination of solubility of polymorphs using differential scanning calorimetry, Cryst. Growth Des. 3 (6) (2003) 991–995. doi:10.1021/cg0340502.